

J. M. García-Aznar · T. Rueberg · M. Doblare

## A bone remodelling model coupling microdamage growth and repair by 3D BMU-activity

Received: 8 March 2004 / Accepted: 17 December 2004 / Published online: 8 June 2005  
© Springer-Verlag Berlin Heidelberg 2005

**Abstract** Bone as most of living tissues is able, during its entire lifetime, to adapt its internal microstructure and subsequently its associated mechanical properties to its specific mechanical and physiological environment in a process commonly known as bone remodelling. Bone is therefore continuously renewed and microdamage, accumulated by fatigue or creep, is removed minimizing the risk of fracture. Nevertheless, bone is not always able to repair itself completely. Actually, if bone repairing function is slower than microdamage accumulation, a type of bone fracture, usually known as “stress fracture”, can finally evolve. In this paper, we propose a bone remodelling continuous model able to simulate microdamage growth and repair in a coupled way and able therefore to predict the occurrence of “stress fractures”. The biological bone remodelling process is modelled in terms of equations that describe the activity of basic multicellular units. The predicted results show a good correspondence with experimental and clinical data. For example, in disuse, bone porosity increases until an equilibrium situation is achieved. In overloading, bone porosity decreases unless the damage rate is so high that causes resorption or “stress fracture”.

### 1 Introduction

Bone’s ability to adapt its internal microstructure and external shape to the surrounding mechanical and physiological environment has been a subject of research and discussion for more than a century. In 1892, Julius Wolff enunciated its famous assumption that directly related bone’s architecture to the directions of principal stresses, which is nowadays known as Wolff’s Law (Wolff 1986). Although this “law” has been considered the fundamental underpinning of bone adaptivity during decades, it has caused much controversy (Cowin 2001). Bone remodelling is the term that describes the relationship between internal bone tissue structure and the mechanical loads that it supports, whereas, bone modelling refers to the laws that define external shape changes as function of the mechanical usage. In this work, we mainly focus on bone remodelling.

Regarding this latter aspect and especially in the last 20 years, many analytical and computational models have been proposed (Huiskes et al. 1987; Carter et al. 1987, 1989; Prendergast and Taylor 1994; Martin 1995; Jacobs et al. 1997; Hart and Fritton 1997; Fernandes et al. 1999; Doblare and García 2002, 2001). Perhaps the first complete consistent model was the *theory of adaptive elasticity* of Cowin and Hegedus (1976). The fundamental underlying assumption was that trabecular bone’s apparent density is controlled by mechanical macroscopic variables, such as strain, and local elastic isotropic constants are only dependent on this apparent density. These assumptions were used by different groups (Hart et al. 1984; Huiskes et al. 1987; Carter et al. 1987, 1989; Beaupré et al. 1990; Weinans et al. 1992) to establish several extensions or specializations, finite element implementations and different practical applications. Bone however is anisotropic. Extensions to anisotropic remodelling have been also proposed in theoretical (Cowin 1986; Luo et al. 1992) and computational versions (Jacobs et al. 1997; Hart and Fritton 1997; Fernandes et al. 1999; Doblare and García 2002,

Research partially supported by Diputación General de Aragón project P-008/2001) and National Network IM3 (Molecular and Multimodal Medical Imaging, Spanish Ministry of Health, Associated Partner, 300+ +, 2003-2005)

J. M. García-Aznar · T. Rueberg · M. Doblare (✉)  
Group of Structural Mechanics and Material Modelling,  
Aragón Institute of Engineering Research (I3A),  
University of Zaragoza, C/María de Luna 5,  
“Agustín de Betancourt” Building, 50018 Zaragoza, Spain  
E-mail: mdoblare@unizar.es  
Tel.: +34-97-6761912  
Fax: +34-97-6762578

2001). More recently, other approaches with different assumptions, such as, remodelling activated by micro-damage have also been presented (Prendergast and Taylor 1994; Martin 1995; Ramtani and Zidi 2001; Doblaré et al. 2004). The interested reader can find additional details in several excellent reviews (Hart 2001; Petermann et al. 1997).

Most of the above models are of phenomenological nature, and explain the net change of bone apparent density by the coordinated and simultaneous activity of osteoblasts and osteoclasts. On the contrary, biologically-based models try to consider both biological and mechanical factors and to include current knowledge about bone cell activity. In this direction some attempts have been recently developed (Huiskes et al. 2000; Hazelwood et al. 2001; Hernandez 2001; Hernandez et al. 2000; Taylor and Lee 2003; Taylor et al. 2004).

Here, we present an extension of these latter to predict both the process of bone remodelling and bone stress fractures, merging and extending concepts from some of them (Hazelwood et al. 2001; Hernandez 2001; Hernandez et al. 2000; Prendergast and Taylor 1994; Martin 1995; Ramtani and Zidi 2001; Doblaré et al. 2004). For example, those models that consider micro-damage accumulation as the activation stimulus, do not take into account the actual biology of the process, well developed for instance by Prendergast and Taylor (1994), Ramtani and Zidi (2001), Doblaré et al. (2004). On the other hand, the approach proposed by Hazelwood et al. (2001) assumes that bone remodelling is activated by disuse and microdamage, including some biological effects such as BMU activity. These authors quantify damage accumulation as the difference between growth and repair. Another biological proposal was successively developed by Hernández (2001) and Hernandez et al. (2000, 2001) that includes biological and metabolic influences on bone adaptation. They analyzed the effect of several biological factors directly related to BMU activity, such as, mineralization period, focal bone balance or activation frequency. However, these last works do not take into account the degradation that damage induces in the mechanical properties of bone and the subsequent modification on the mechanical stimuli, thus making them incomplete for a full understanding of the coupling mechanism between damage accumulation (purely mechanical) and biological bone response. In fact, the determination of the rates of damage accumulation and repair are crucial to prevent stress fractures and to control bone mass net production.

We have focused here on exploring the coupling effect between fatigue damage removal/accumulation and biological events that occur in bone remodelling. With this aim we have formulated a continuum damage theory able to predict damage growth and the subsequent degradation of the elastic modulus of bone under cyclic loading. This theory is coupled with a bone remodelling approach based on previous existent biological formulations (Hernandez 2001; Hernandez et al. 2000, 2001; Hazelwood et al. 2001). This combined theory has been

used to analyze the influence of different mechano-biological factors in a coupled way, obtaining novel conclusions about bone remodelling.

## 2 Bone remodelling theory

The model proposed in this work formulates the adaptation of the internal structure of bone in terms of bone volume fraction, damage level and mineralization degree. All of them evolve in response to the mechanical environment including the current damage state (Fig. 1).

In the following subsections, each component of the model is explained in detail. We firstly introduce the internal scalar variables that characterize bone tissue as a structural material. Next, the time evolution of these variables will be determined as functions of the different mechanical and biological factors.

### 2.1 Definition of internal scalar variables

Bone is a composite of tissue matrix and pores, mainly filled with marrow, blood vessels, and nerves. However, the mechanical influence of these latter components is negligible with respect to the much stiffer matrix. From the structural point of view, bone properties can be quantified through the subdivision  $V_T = V_B + V_V$ , where  $V_B$  and  $V_V$  refer to the bone matrix tissue and void or pore subvolumes, respectively.  $V_T$  denotes the total reference volume of analysis. The tissue matrix is composed of inorganic (mineral) and organic (mainly collagen) parts, represented by the volume measures  $V_M$

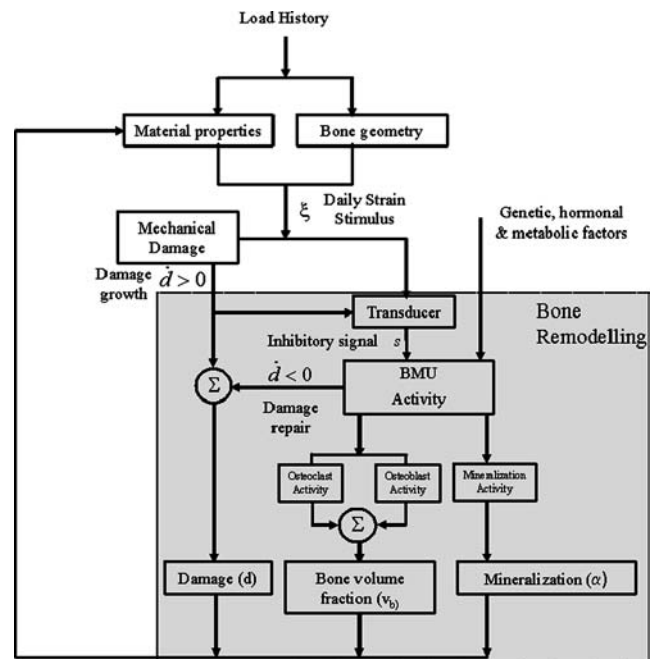


Fig. 1 Schematic representation of the bone remodelling algorithm proposed

and  $V_O$ , respectively. Furthermore, we assume a certain volume of tissue to be damaged ( $V_D$ ) (this volume is a measure of the density of microcracks that we consider randomly and isotropically distributed causing a reduction of the mechanical properties), such that

$$V_T = V_B + V_V = V_M + V_O + V_D + V_V. \quad (1)$$

The establishment of the time evolution of these subvolumes is the main objective of an isotropic bone remodelling theory. With this objective, as most other models, we introduce the independent variable *bone volume fraction*  $v_b$ , as

$$v_b = \frac{V_B}{V_T} \quad (2)$$

which can be measured experimentally and has a significant impact on the overall mechanical behaviour (Hernandez et al. 2001). Porosity  $p$  can be directly expressed as

$$p = \frac{V_V}{V_T} = 1 - v_b. \quad (3)$$

The second independent variable characterizes the degree of mineralization and is called *ash fraction*,  $\alpha$  (Hernandez 2001; Hernandez et al. 2001). It is defined as the ratio between the mineral mass  $m_M$  (also termed ash mass, since it results after the organic constituents have been evaporated in a furnace) and the dry mass, which is the sum of mineral and organic mass,  $m_d = m_M + m_O$ . Hence,

$$\alpha = \frac{m_M}{m_M + m_O} = \frac{\rho_M V_M}{\rho_M V_M + \rho_O V_O}, \quad (4)$$

where  $\rho_M$  and  $\rho_O$  refer to the densities of the mineral and organic components, respectively.

A third independent variable is necessary to quantify the damage state. Damage intensity can be evaluated by the macroscopic mechanical degradation or as a microscopic measure of the density of internal microcracks. Both variables are physically related and it has been experimentally determined in bone tissue and correlated (Burr et al. 1998). Nevertheless, we have to keep in mind that there is not yet a fully quantitative relation between physical damage and degradation (Jepsen et al. 2001). We however distinguish between these two concepts. First, we define a dimensionless variable  $h$  that quantifies the microcrack density in the reference volume

$$h = \frac{V_D}{V_T}. \quad (5)$$

Next, we introduce the macroscopic variable  $d$  as that experimentally related to the loss of stiffness by means of this expression

$$d = 1 - \frac{E}{E_0}, \quad (6)$$

where  $E_0$  corresponds to a reference value of the elastic modulus associated to an ideal undamaged material (Jepsen et al. 2001; Davy and Jepsen 2001; Pattin et al. 1996; Zioupos and Currey 1998; Burr et al. 1998). This variable corresponds to the continuum damage variable usually used in the isotropic theory of Continuum Damage Mechanics (Lemaitre and Chaboche 1990; Simo and Ju 1987; Davy and Jepsen 2001), which is thereby restricted to the interval  $[0, 1]$ .

As it has been previously indicated the relationship between microcrack density  $h$  and stiffness degradation  $d$  is not fully understood and may depend on many factors, such as, load state, porosity, type of bone and so on. Only particular correlations have been determined, as for example, that proposed by Burr et al. (1998) that obtained a linear relationship between stiffness loss and crack effective area for intact canine femurs subjected to bending.

Therefore, using this result as a first approach, we assume a linear relationship between  $h$  and  $d$

$$h = f(d) = kd \quad (7)$$

with  $k$  a constant that has to be experimentally determined.

Note that the *apparent density*  $\rho$ , the basic variable in most bone remodelling models (Beaupré et al. 1990; Carter et al. 1989, 1987; Huiskes et al. 1987; Jacobs et al. 1997; Weinans et al. 1992; Doblaré and García 2002, 2001), can be related to the bone volume fraction by  $\rho = \rho_t (v_b - h)$ , where  $\rho_t$  is the real tissue density, i.e., the density of bone with null porosity  $\rho_t = \rho_M V_M + \rho_O V_O / (V_M + V_O)$ . This tissue density depends on the degree of mineralization. A linear approximation relating tissue density and ash fraction, in good correlation with experimental data, was given by Hernandez (2001) and Hernandez et al. (2001) as  $\rho_t = 1.41 + 1.29\alpha$  (in  $\text{g/cm}^3$ ). In fact, in several experimental outcomes (Hernandez 2001; Hernandez et al. 2001; Keller 1994), bone elastic properties showed a better correlation with the bone volume fraction  $v_b$  and ash fraction  $\alpha$  than with the apparent density  $\rho$ .

The bone material stiffness is determined in the isotropic case by the Young's modulus  $E$  and Poisson ratio  $\nu$ . We have used the relation proposed by Hernandez (2001) and Hernandez et al. (2001), but taking into account the loss of stiffness due to damage, such that

$$E = 84370 v_b^{2.58} \alpha^{2.74} (1 - d) = \hat{E} v_b^\beta (1 - d) \text{ MPa} \quad (8)$$

being  $\hat{E}$  the elastic modulus of bone with null porosity and undamaged for a given ash fraction. Additionally, we have assumed that the Poisson ratio is set to a constant value of  $\nu=0.3$ , since its variation is not very important (Martin et al. 1998).

## 2.2 Mathematical description of BMU activity

It is commonly accepted that bone remodelling is carried out by the so-called *basic multicellular units* (BMUs)

composed by tissue-resorbing osteoclasts and tissue-forming osteoblasts working in a coupled way. These cell units proceed in a strict order at a fixed point: after being activated, they first resorb bone tissue for a time interval named *resorption period* ( $T_R$ ), and, after a *reversal time* ( $T_I$ ), the *formation period* ( $T_F$ ) starts. This sequence has been originally termed as *A-R-F sequence* (activation, resorption, formation) by Frost (1964). The lifespan of a BMU is denoted by  $\sigma_L$  and refers to the time during which the first appearing osteoclasts are active. This is a useful definition, since  $\sigma_L$  is directly related to the maximum distance that a BMU travels (for example, the average length of an osteon) by means of its progression speed  $v_{BMU}$ , the so-called *BMU-rate*. Note that these measures belong to a 3D histomorphometry and therefore consider the spatial and time progression in a 3D space.

Both processes of resorption and formation are not only coupled but also take place continuously, even in remodelling equilibrium. Their main goals are considered to be microdamage removal and calcium provision other than mechanical adaptation. The rate of change of bone volume fraction is expressed as:

$$\dot{v}_b = \dot{v}_F - \dot{v}_R, \quad (9)$$

where  $\dot{v}_F$  and  $\dot{v}_R$  are the rates of variation of volume due to formation and resorption, respectively. In remodelling equilibrium  $\dot{v}_b = 0$ , so formed and resorbed tissue rates become equal.

These changes in bone volume fraction are functions of the number of BMUs currently active that will be represented by the BMU-density  $N_{BMU}$ , defined as the number of BMUs per reference volume (BMU  $s/mm^3$ ). Once activated, a BMU moves through a distance  $L_{BMU} = \sigma_L v_{BMU}$ . Each of these rates of bone volume fraction can therefore be expressed as

$$\dot{v}(t) = \int_0^{L_{BMU}} \left( \int_{t'-\sigma_L}^{t'} \dot{N}_{BMU}(t'') dt'' \right) \dot{A}(x) dx, \quad (10)$$

where  $dx$  is measured along the direction of progression of a BMU,  $\int \dot{A}(x) dx$  is the rate of variation of volume

per unit length at a specific coordinate  $x$  along the progression path, and  $\int_{t'-\sigma_L}^{t'} \dot{N}_{BMU}(t'') dt''$  determines the number of active BMUs at the considered time  $t'$ .

We assume that the rate of remodelling through the transverse direction, i.e. normal to the main direction of progression, is constant and independent of the spatial variable  $x$ . Distinguishing between resorption and formation, this transverse remodelling rate will be expressed as

$$\dot{A}(x) dt = \begin{cases} \frac{A_{BMU}}{T_R} f_c & \text{if resorption} \\ \frac{A_{BMU}}{T_F} f_b & \text{if formation} \end{cases} \quad (11)$$

with  $T_R$  and  $T_F$  the resorption and formation periods, respectively,  $f_b$  and  $f_c$  normalized variables between 0 and 1 that represent the level of osteoblast and osteoclast activity, respectively, and  $A_{BMU}$  the total cross-sectional area of a BMU. Since the cross section geometries of cortical and cancellous BMUs are completely different, we considered different  $A_{BMU}$  for each type of tissue (see Fig. 2).

Furthermore,  $dx$  is directly expressed in terms of the rate of progression of a BMU by  $dx = v_{BMU} dt$ . If we combine Eq. (10) to Eq. (11), the volume of removed/refilled bone can be written as

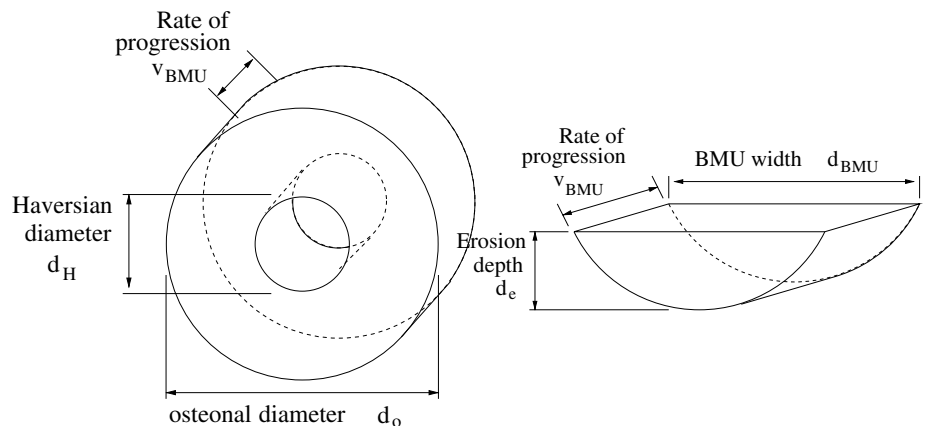
$$\dot{v}_F(t) = \int_{t-T_R-T_I-T_F}^{t-T_R-T_I} \left( \int_{t'-\sigma_L}^{t'} \dot{N}_{BMU}(t'') dt'' \right) \frac{A_{BMU}}{T_F} f_b(t') v_{BMU} dt', \quad (12a)$$

$$\dot{v}_R(t) = \int_t^{t-T_R} \left( \int_{t'-\sigma_L}^{t'} \dot{N}_{BMU}(t'') dt'' \right) \frac{A_{BMU}}{T_R} f_c(t') v_{BMU} dt'. \quad (12b)$$

Equations (12) describe the changes in bone volume fraction at time  $t$  in terms of the changes in BMU-density which took place in the recent history.

The other factor that controls the amount of bone tissue removed or formed is the balance between

**Fig. 2** A model of the tissue volume unit that a single BMU remodels in cortical (*left*) and cancellous (*right*) bone tissue per time unit (adapted from Hernandez 25)



osteoblast and osteoclast activity,  $f_{bb} = (f_b/f_c)$ , normally known as *focal bone balance* (Hernandez 2001; Hernandez et al. 2000). We assume that this balance is directly related to the mechanical stimulus  $\xi$  (Rubin et al. 2001; Huiskes et al. 2000; Jacobs et al. 1997; Doblaré and García 2002) and to the age (Carter and Beaupré 2001; Martin et al. 1998). In this work, the mechanical influence is defined in terms of a scalar quantity following the idea proposed by Mikic and Carter (1995), which represents the daily strain history and, therefore, depends on the strain level and the number of cycles for each load case  $i$

$$\xi = \left( \sum_i N_i \bar{\varepsilon}_i^m \right)^{\frac{1}{m}}, \quad (13)$$

where  $N_i$  denotes the number of load cycles per day,  $\bar{\varepsilon}_i$  the level of the applied strain for each load case  $i$  and  $m$  the stress exponent that weights the relative importance of the strain magnitude and the number of load cycles in the mechanical stimulus. Typically,  $m=4$ , which was determined from experimental data for cortical and cancellous bone (Whalen et al. 1988). The used strain functional has been defined as

$$\bar{\varepsilon} = \sqrt{\frac{2U}{E}} \quad (14)$$

with  $U = \frac{1}{2} \varepsilon : \mathbf{C} : \varepsilon$  the strain energy density.

Additionally, we propose a piece-wise linear model to relate  $f_{bb}$  with the unbalanced stimulus  $\xi - \xi^*$  (Beaupré et al. 1990; Huiskes et al. 1987; Jacobs et al. 1997; Jacobs 1994) (Fig. 3). As in many other models (Carter 1984; Huiskes et al. 1987; Beaupré et al. 1990; Jacobs et al. 1997; Jacobs 1994; Doblaré and García 2002; Tsubota et al. 2002), we assume the existence of a *dead zone*, i.e., a certain interval around the reference stimulus  $\xi^*$  in which  $f_{bb}$  maintains its equilibrium value  $f_{bb} = 1$ . The half-width of this dead zone is denoted by  $w$ . Furthermore,  $f_{bb}$  tends linearly to its maximum (or minimum value) in the region  $\xi - \xi^* \in (w, w + v)$  ( $\xi - \xi^* \in (-w, -w - v)$ ), such that any value of  $\xi$  greater than  $\xi^* + w + v$  (smaller than  $\xi^* - w - v$ ) will be assigned  $f_{bb} = f_{bb, \max}$  ( $f_{bb, \min}$ ). In this sense, a stimulus  $\xi > \xi^* + w$  causes  $f_{bb} > 1$ , so the amount of tissue formed is greater than the resorbed. Equivalently,  $\xi < \xi^* - w$

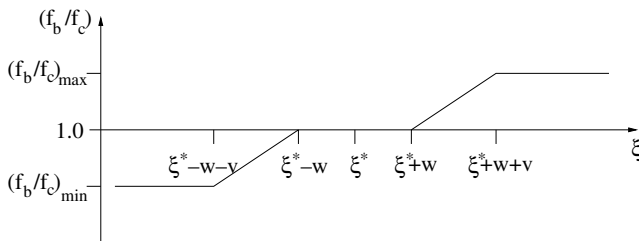


Fig. 3 Bone focal balance Model for the focal bone balance

causes more resorption than formation,  $f_{bb} < 1$ . As shown in Fig. 3, we assume the cell activity to be limited, such that a high stimulus  $\xi > \xi^* + w + v$  does not result in an excessive bone volume change which is outside experimental validation. In fact, the effect of the focal bone balance is not considered in cortical bone during bone formation due to insufficient space for bone refilling, i.e.,  $f_{bb} = 1.0$  for any  $\xi > \xi^* + w$ .

The reference stimulus  $\xi^*$  typically has a value of  $\xi^* = 2.5 \times 10^{-3}$  (equivalent to a tissue level stress of 50 MPa in cortical bone, cf. Beaupré et al. 1990). But this value seems to be only applicable to weight-bearing bones (e.g., femur, tibia), whereas fewer charged bones (e.g. protective flat bones such as skull or scapula) cannot be subjected to such a high value. These different values in different types of bones could be explained by assuming that the reference stimulus  $\xi^*$  is not constant, but dependent on the load history, modifying its value in an adaptative way. This idea is similar to the concept of cellular accommodation proposed by Turner (1999). We therefore assume that the reference stimulus  $\xi^*$  adapts to the applied stimulus  $\xi$ , using this asymptotic function

$$\xi^*(\xi, t) = \xi - (\xi - \xi_0^*)e^{-\phi t}, \quad (15)$$

where  $\xi_0^*$  denotes the initial reference stimulus and the parameter  $\phi$  controls the velocity of adaptation. The main consequence of Eq. (15) is that a permanently low or high stimulus value does not yield excessive remodelling. This also allowed us to extend the applicability of our method to a variety of bone types, which has not been incorporated in other models.

### 2.3 Balance of bone mass

In order to understand the bone mass remodelling, we consider the local statement of balance of mass for the porous matrix in the initial configuration:

$$\frac{\partial \rho}{\partial t} = \frac{\partial \rho'}{\partial t} (v_b - h) + \rho' \frac{\partial v_b}{\partial t} - \rho' \frac{\partial h}{\partial t} = \Pi^b, \quad (16)$$

where  $\Pi^b$  is the rate at which mass per unit volume is added to or removed from the bone volume matrix. Each term of this expression determines how bone mass adapts. The first term describes how the deposited osteoid is mineralized, the second defines the evolution caused by bone mass matrix deposition or resorption due to BMU activity and the third term defines the effect of damage evolution.

For a better comprehension of the evolution of all these variables is adequate to analyze the events that bone senses: damage growth, bone resorption and bone formation. Next, each of these processes are explained and described by means of the corresponding equations that define the evolution of all internal variables.

### 2.3.1 Damage growth

Bone tissue is often subjected to cyclic or fluctuating loads that causes an accumulation of microstructural damage, which may culminate in the formation and growth of macroscopic cracks. We consider this process to be uncoupled from production of bone mass ( $\pi^b=0.0$ ) and mineralization ( $\partial\rho^t/\partial t=0$ ). Therefore, from the balance of bone mass equation (16), we can see that damage growth leads to an increase of bone volume fraction:

$$\frac{\partial h}{\partial t} = \frac{\partial v_b}{\partial t}. \quad (17)$$

Fatigue behaviour of bone subjected to cyclic loads has been intensively studied (Pattin et al. 1996; Jepsen et al. 2001; Burr et al. 1998; Zioupos and Currey 1998; Lee et al. 2000) through the measure of elastic modulus degradation ( $d$ ). Therefore, the evolution of the micro-crack density ( $h$ ) is completely determined by means of the relationship 7 and the evolution of  $d$ :

$$\frac{\partial h}{\partial t} = k \frac{\partial d}{\partial t}. \quad (18)$$

Although in the outcome of bone fatigue experiments underlies a great statistical variety, a common pattern can be detected and fatigue damage growth can be formulated as

$$\frac{\partial d}{\partial N} = G(d, \bar{\epsilon}) \quad (19)$$

with a different function  $G$  for tension and compression (Pattin et al. 1996) states. Therefore, we have defined two different evolution laws:

$$\frac{\partial d_c}{\partial N} = G_c(d, \bar{\epsilon}) = \frac{C_1}{\gamma_1} e^{\gamma_1 d} \bar{\epsilon}^{\delta_1} \quad \text{in compression} \quad (20a)$$

$$\frac{\partial d_t}{\partial N} = G_t(d, \bar{\epsilon}) = \frac{C_2}{C_3 \gamma_2} (1-d)^{1-\gamma_2} e^{-C_3(1-d)^{\gamma_2}} \bar{\epsilon}^{\delta_2} \quad \text{in tension} \quad (20b)$$

with  $C_j$ ,  $\gamma_j$  and  $\delta_j$  parameters that depend on the applied strain level  $\bar{\epsilon}$  defined in Eq. (14). Integration of Eq. (20) yields

$$d_c = -\frac{1}{\gamma_1} [\ln(1 - C_1 \bar{\epsilon}^{\delta_1} N)], \quad (21a)$$

$$d_t = 1 - \gamma_2 \sqrt{\frac{1}{C_3} \ln(e^{C_3} - C_2 \bar{\epsilon}^{\delta_2} N)}. \quad (21b)$$

On the other hand, fatigue life expectation is typically of the form

$$N_f = C \bar{\epsilon}^\delta. \quad (22)$$

Correlating (22) with experimental results obtained by Pattin et al. (1996), we get

$$N_f = \frac{9.333}{(E/E^*)^{\bar{\epsilon}^{10.3}}} \quad \text{in compression} \quad (23a)$$

$$N_f = \frac{1.445}{(E/E^*)^{\bar{\epsilon}^{14.1}}} \quad \text{in tension} \quad (23b)$$

with  $E^*$  the reference modulus of elasticity used to perform the fatigue tests and  $E$  the current Young's modulus of the bone specimen supporting  $\bar{\epsilon}$ .

Setting now  $d=1$  in one of the Eqs. (21) and solving for  $N=N_f$ , we can determine the different parameters involved in Eq. (20), resulting into the following approximate values

$$\begin{aligned} \delta_1 &= 10.3; \quad \gamma_1 = -5.238 \left( \frac{E}{E^*} \bar{\epsilon} - 6100 \right) 10^{-3} + 7; \\ C_1 &= \frac{1 - e^{-\gamma_1}}{9.333 \times 10^{40}} \end{aligned} \quad (24a)$$

$$\begin{aligned} \delta_2 &= 14.1; \quad \gamma_2 = -0.018 \left( \frac{E}{E^*} \bar{\epsilon} - 4100 \right) + 12; \\ C_2 &= \frac{e^{C_3} - 1}{1.445 \times 10^{53}}; \quad C_3 = -20.; \end{aligned} \quad (24b)$$

for compression and tension, respectively. The qualitative shapes of these functions for different levels of strain are shown in Fig. 4 in a normalized diagram, that represents the elastic modulus reduction.

Moreover, we assume that in case of cortical bone, the quotient ( $E/E^*$ ) is equal to 1, because all experiments performed by Pattin et al. (1996) used cortical bone. However, in the case of trabecular bone, we have used the Eq. (8) and  $E^* = E(v_b = 0.95; d = 0.0; \alpha = 0.69)$ .

### 2.3.2 Bone resorption and damage repair

Bone can repair itself. In this sense, the main assumption we used is that the damaged subvolume  $V_D$  is uniformly distributed in the bone volume,  $V_B$ . Therefore, the rate of change of the crack density  $h$  due to remodelling would be

$$\frac{\partial h}{\partial t} = -\dot{v}_R \frac{h}{v_b}, \quad (25)$$

where  $\dot{v}_R$  is the bone volume digested by osteoclasts in active BMUs.

As during bone resorption, without additional mineralization, the real tissue density does not change ( $\partial\rho^t/\partial t=0$ ), the total subtracted bone ( $\pi^b$ ) can be determined using the equation of mass balance 16:

$$\pi^b = -\rho^t \dot{v}_R \left( 1 - \frac{h}{v_b} \right). \quad (26)$$

### 2.3.3 Bone formation and mineralization

When bone tissue is deposited, the newly formed tissue is primarily collagen. As time proceeds this tissue calcifies

and the volume of osteoid is converted into mineral. Over the first few days of mineralization, crystals appear throughout the mineralized bone, occupying the space of water. This transformation happens rapidly at the

As the degree of mineralization is not correlated with bone volume fraction, an averaged ash fraction  $\bar{\alpha}$  is introduced, that takes into account the different mineralization stages of the adapted bone

$$\bar{\alpha}(t) = \frac{(v_{b,0} - h_0)\alpha(t) + \int_0^t ((\dot{v}_F(\tau) - h(\tau))\alpha(t - \tau) - (\dot{v}_R(\tau) - h(\tau))\bar{\alpha}(\tau))d\tau}{v_b(t) - h(t)}. \quad (28)$$

beginning and retards like a saturation process. Mineralization is therefore generally divided into two phases, the fast primary phase which proceeds within a few days (Parfitt 1983) yields at about 60% of the maximum mineral content, while the slow secondary phase takes years. In this work, we have assumed that the primary phase occurs immediately. For the secondary phase and employing the ash fraction  $\alpha$  as the measure of the degree of mineralization, we propose an exponential evolution

$$\alpha(t) = \alpha_{\max} + (\alpha_0 - \alpha_{\max})e^{-\kappa t}, \quad (27)$$

where  $\alpha_0$  denotes the ash fraction resulting from the primary phase and  $\alpha_{\max}$  its maximum physiological value. The constant  $\kappa$  determines the velocity of the process (Fig. 5).

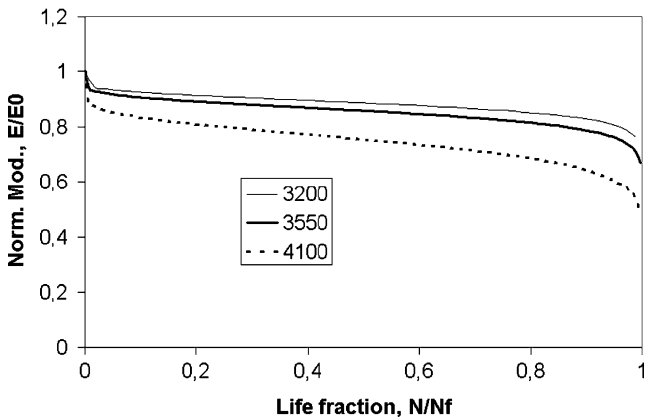
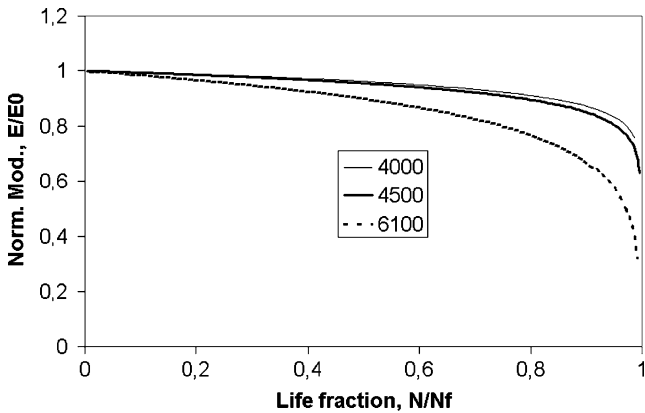


**Fig. 4** Qualitative shape of bone damage  $d$  is a function of the relative cycle number  $N/N_f$  in compression (*top*) and tension (*bottom*) for different levels of compression: 4,000, 4,500 and 6,100  $\mu\epsilon$ , and tension: 3,200, 3,550 and 4,100  $\mu\epsilon$

This averaged ash fraction thus consists of the evolution of the mineral content of the initial bone volume fraction  $v_{b,0}$ , the contribution of the newly formed tissue (convolution integral) and an approximation of the reduction by resorption (since it is not known which ash fraction the resorbed tissue possessed, the average  $\bar{\alpha}$  is used). In order to reduce the numerical effort, an approximate expression for the averaged ash fraction at time  $t + \Delta t$  is established as

$$\bar{\alpha}(t + \Delta t) = \frac{\bar{\alpha}(t)((v_b(t) - h(t))e^{-\kappa\Delta t} - \Delta v_R) + \Delta v_F \alpha_0}{v_b(t + \Delta t) - h(t + \Delta t)} + \frac{\alpha_{\max}(1 - e^{-\kappa\Delta t})(v_b(t) - h(t))}{v_b(t + \Delta t) - h(t + \Delta t)} + \frac{(1 - e^{-\kappa\Delta t}) \int_0^t (\dot{v}_R - \dot{h})(\alpha_{\max} - \bar{\alpha}(\tau))d\tau}{v_b(t + \Delta t) - h(t + \Delta t)}, \quad (29)$$

where  $\Delta v_F$  and  $\Delta v_R$  approximate the amounts of tissue formed and resorbed, respectively, in the time interval  $[t, t + \Delta t]$ . Except for the remaining integral, which has to be stored separately, all values in Eq. (29) are known at each time increment.

Therefore, we define the average real tissue density through the average mineralization degree using the expression  $\bar{\rho}_t = 1.41 + 1.29\bar{\alpha}$ .

And thus, the total mass production in this case would be:

$$\pi^b = [v_b(t + \Delta t) - h(t + \Delta t)]\bar{\rho}_t(t + \Delta t) - [v_b(t) - h(t)]\bar{\rho}_t(t). \quad (30)$$

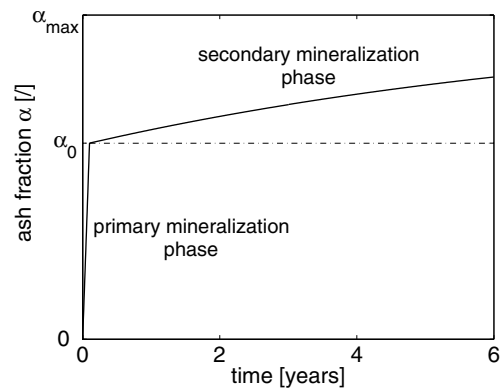


**Fig. 5** The evolution of the ash fraction in time.  $\kappa$  has been chosen such that 50% of the second mineralization is achieved after 6 years

## 2.4 Balance of BMUs

Changes in the BMU-density  $N_{\text{BMU}}$ , i.e. changes in the number of BMUs currently active, result either from exceeding their life span  $\sigma_L$  in form of a decrease in number, or from the origination of new BMUs in form of an increase. Whereas the former event (also referred to as *apoptosis*) takes place “automatically”, the latter is controlled by the *origination frequency*  $f_{\text{or}}$  (or birthrate) and the available surface area per reference bone volume  $S_v$  in such a way that

$$\frac{\partial N_{\text{BMU}}}{\partial t} \left( \frac{N_{\text{BMU}}}{\text{mm}^3 \text{day}} \right) = \Pi_{\text{BMU}} = f_{\text{or}} S_v \quad (31)$$

The dependence of the BMU birthrate on the surface density,  $S_v$  indicates that bone remodelling only occurs on tissue surfaces. The available surface directly depends on porosity. Martinn (1984) for example, correlated both by a quintic polynomial.

The second factor that determines the occurrence of new BMUs is the origination frequency, which is controlled by different metabolic and mechanical factors. It is known, for instance, from experimental results (Rubin et al. 2001; Gross and Rubin 1995; Li et al. 1990; Takata and Yasui 2001; Jaworski and Uthoff 1986) that bone volume fraction decreases in a state of disuse, while it has been suggested that microdamage caused by fatigue or overloading activates remodelling in order to repair those damaged regions (Martin 2003a, b; Bentolila et al. 1990; Mori and Burr 1993; Verbogt et al. 2000).

Here, we follow the inhibitory theory proposed by Martin (2000). In this theory, it is assumed that bone lining cells are inclined to activate BMU activity and therefore bone remodelling, except when they receive an inhibitory signal from the osteocytic network. Therefore, we propose

$$f_{\text{or}} = f_{\text{bio}}(1 - s), \quad (32)$$

where  $f_{\text{bio}}$  is a certain biological factor and  $s$  the normalized level (between 0 and 1) of the inhibitory signal.

This signal is generated by the strain and felt by osteocytes. Any perturbation in the reception of such signal causes a certain degree of activation. This alteration may be due either to a low strain level or to its anomalous transmission through the cellular network, for example due to the existence of microcracks that disrupt the network connectivity. Therefore we propose that this inhibitory signal  $s$  depends on a variable characteristic of the mechanical usage  $\xi$  and the damage level  $d$  by means of:

$$s(\xi, d) = \frac{\xi}{\xi + c} (1 - d)^a \quad (33)$$

with  $c$  and  $a$  model parameters that define the transduction role of these purely mechanical variables,  $\xi$  and damage  $d$  (see Fig. 6). This expression fulfils all the

necessary requirements, such as,  $s(0, d) = 0$  for any  $d$ , i.e., no signal will be generated in the pathological case of total disuse, and  $s(\xi, 1) = 0$  for any  $\xi$ , i.e., in a state of full damage, transmission is not possible. Finally,  $\lim_{\xi \rightarrow \infty} s(\xi, 0) = 1$ , since the signal is normalized to the interval  $[0, 1]$ .

## 3 Results

In this section we initially perform a parametric analysis in order to determine the influence of each variable in the global bone response. Next this same theory is applied to study a common problem in biomechanics as the bone adaptation consequence of a hip implant replacement.

### 3.1 Validation of the model

To illustrate the biophysical significance of the remodelling model just outlined we consider initially an 1D test. In this simple problem, the influence and interaction among the main biological and mechanical variables is analyzed by means of a sensitivity analysis under different conditions of constant stress and strain. The parameters used are given in Table 1 and 2. All test calculations simulated the behaviour in 3,000 days. The initial state was assumed to be in equilibrium, i.e., with a constant birthrate and a focal bone balance  $f_{\text{bb}} = 1.0$ . In fact, the initial values were chosen as if a stimulus of  $\xi = \xi_0^*$  had been applied before the beginning of the calculation, for time  $t < 0$ . Therefore, the initial number of BMUs  $N_{\text{BMU}0}$  is uniquely determined by the expression:

$$N_{\text{BMU}0} = f_{\text{bio}}(1 - s(\xi_0^*, d_0)) S_v(\rho_0), \quad (34)$$

where  $\rho_0$  is the initial apparent density and  $d_0$  the initial damage.

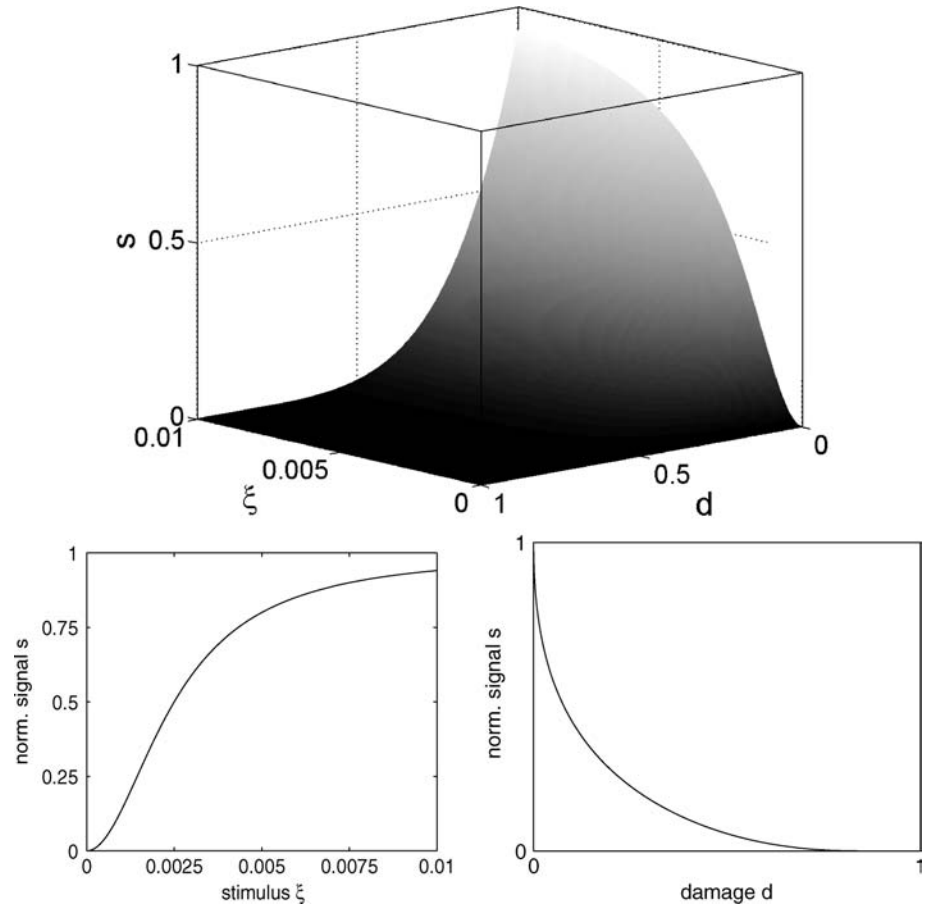
A time step of 1 day was chosen for the analysis in order to reduce the computational cost of all simulations.

#### 3.1.1 Influence of elastic modulus degradation

As we have presented in the Introduction section, this model is able to predict both bone remodelling and stress fractures. Next we show a simple example in which we study the significance of considering the degradation of elastic modulus when microdamage is produced ( $d > 0$ ) (see Eq. 8). If we apply a high constant stress level of 34 MPa on cortical bone with an initial density of 2.05 g/cm<sup>3</sup> we can observe how the model response is completely different depending on the consideration or not of the elastic modulus deterioration (see Fig. 7). In fact, the consideration of the elastic modulus reduction allowed us to predict the appearance of a stress fracture. This is direct consequence of a bone remodelling



**Fig. 6** Normalized signal level as a function of the strain-based stimulus  $\xi$  and the damage state  $d$  (Eq. (33) with  $c=0.0025$  and  $k=5$ ). *Top*: 3D plot of the scalar field  $s(\xi, d)$ . *Bottom*: curves  $s(\xi, 0)$  and  $s(\infty, d)$



repairing slower than damage increasing. On the contrary, in the case of not considering the effect of microdamage on the elastic modulus, the model predicts that bone is able to repair itself and no fracture is predicted.

Therefore, we show in this work with this simple example, that the addition of this hypothesis is very important for studying and understanding the combining process of microdamage growth and repair.

### 3.1.2 Influence of the strain level

In Fig. 8, the evolution of the bone volume fraction is presented for different initial densities (2.05, 1.0 and 0.5 g/cm<sup>3</sup>) under constant strain, corresponding to different states of strain level: equilibrium ( $\xi = \xi^*_0$ ), overload ( $\xi = 2\xi^*_0$ ), high overload ( $\xi = 7\xi^*_0$ ) and disuse ( $\xi = 0$ ). A fixed number of cycles per day (10,000 cycles/day) has been applied in all the cases. For cortical bone (initial density of 2.05 g/cm<sup>3</sup>) the model responds with a slight increase in bone volume fraction for overload, with a small decrease in the case of high overload due to microdamage accumulation and a higher reduction in case of disuse. For cancellous bone (initial density of 1.0 or 0.5 g/cm<sup>3</sup>) a slight increase in bone volume fraction is also produced under overload and high overload. This increase is higher for greater loads. In the case of disuse,

bone volume fraction decreases. In all the situations analyzed, a stable equilibrium situation is achieved. Since the applied strain was held constant—and therefore the applied stimulus—, convergence was attained when the reference stimulus  $\xi^*$  becomes (cf. Eq. 15) close enough to the applied stimulus, i.e.,  $|\xi - \xi^*| < w$ , being  $w$  the half-width of the dead zone. Figure 8 shows the evolution of the remodelling increments  $\Delta v_F$  and  $\Delta v_R$  due to formation and resorption, respectively. In equilibrium, these values evidently coincide with a constant non-zero value.

As it has been previously remarked, microdamage accumulation is produced under high overload causing bone resorption, especially in cortical bone. In Fig. 9a we can observe how damage accumulation is clearly non-linear with respect to the number of cycles, since damage is continuously being repaired. On the contrary, in trabecular bone, damage is very low, so remodelling is basically not activated (see Fig. 9b) and damage remains practically unrepaired.

### 3.1.3 Effect of parameter $c$ that controls the influence of mechanical stimulus $\xi$ on the inhibitory signal $s$

The model proposed clearly depends on load history. The inhibitory signal  $s$  is the variable that actually controls bone adaptative response and this variable is mainly determined by the load history through  $\xi$  and the

**Table 1** Values assigned to the different parameters of the model

Parameter	Nominal value	Values examined in this work	
General parameters			
$N$	Number of daily load cycles	10,000	5,000–20,000
$m$	Weighting exponent	4	
$\xi_0^*$	Initial equilibrium stimulus	0.0025	
$w$	Half-width of the dead zone	$0.2\xi_0^*$	
$v$	Linear transition zone	$0.2\xi_0^*$	
$f_{bb,max}$	Maximal bone focal balance	1.0	1.2–1.5
$f_{bb,min}$	Minimal bone focal balance	1.0	0.8–0.5
$\phi$	Accommodation velocity parameter	$0.002 \text{ days}^{-1}$	$0.0 - 0.000001 - 0.02$
$c$	Strain activation curve parameter	$\xi_0^*$	$0.000001 \xi_0^* - 0.1 \xi_0^* - 10. \xi_0^* - 1000000. \xi_0^*$
$a$	Damage activation exponent	10	0–50
$k$	Relates microcrack density and elastic modulus reduction	0.00034	
$f_{bio}$	Biological frequency factor	0.03	0.001–0.5–0.01–0.05–0.1–0.2
$d_0$	Initial damage	0.0	
Mineralization			
$\alpha_{ini}$	Initial ash fraction	0.6	
$\alpha_0$	Minimal ash fraction	0.45	
$\alpha_{max}$	Maximal ash fraction	0.7	
$\kappa$	Secondary mineralization period	6 years	1–9–16
Time spans and BMU-geometry			
$T_R$	Resorption period	60 days	
$T_I$	Reversal period	56 days	
$T_F$	Formation period	175 days	
$\sigma_L$	BMU lifespan	100 days	
$d_o$	Osteonal diameter	0.076 mm	
$d_H$	Haversian diameter	0.0145 mm	
$d_e$	Erosion depth	0.0491 mm	
$d_{BMU}$	BMU width	0.152 mm	
$v_{BMU}$	BMU rate	0.01 mm/day	

Nominal values refer to the parameters chosen for the femur model

**Table 2** Variables that control the model and are updated at each time step

State variables			
$v_b$	Bone volume fraction	$d$	Continuum damage variable
$\bar{\alpha}$	Averaged ash fraction	$\xi^*$	Reference stimulus
$\dot{N}_{BMU}$	BMU density		
Intermediate variables			
$\bar{\epsilon}$	Strain measure	$\tilde{d}$	Auxiliary damage variable
$\xi$	Applied stimulus	$f_{or}$	Origination frequency
$S_V$	Available tissue surface	$s$	Norm. signal level
$\dot{v}_R$	Change due to resorption	$\dot{v}_F$	Change due to formation

Note that  $\dot{N}_{BMU}$  is stored with its history

damage level  $d$  (see Eq. (33)). But, at the same time, the influences of these variables is modulated through parameters  $c$  and  $a$ , respectively.

In this section we analyze the influence of parameter  $c$  in the final bone response, fixing the initial apparent density ( $\rho_0 = 2.05 \text{ g/cm}^3$ ) and initial damage ( $d_0 = 0.0$ ) under two different loading conditions: disuse and high overload under constant strain. We have performed a parametric analysis, using different values of  $c$  ( $0.000001-0.1-1-10-1000000. \xi_0^*$ ). From Fig. 10a we can conclude that, under disuse, a high value of  $c$  delays bone resorption, whereas for increasing  $c$  the resorbed bone volume fraction becomes lower. For strong overload we observe that, except for non-physiological high values of  $c$ , bone resorption is always obtained (Fig. 10b). For  $c > 1$  we get maximum bone resorption, while for  $c < 1$  bone resorption becomes higher for lower values of  $c$ . Moreover, for very low values of  $c$ , initial bone formation is never produced.

### 3.1.4 Impact of parameter $a$ that controls the influence of damage level in the inhibitory signal $s$

The stimulus that controls bone response is dependent through Eq. (33) on both load history and damage level. How damage influences the disruption of the inhibitory transmitted signal is currently one of the most active research fields in this area (Cowin and Moss 2001; Noble 2003; Martin 2003a; Taylor et al. 2003). In this work, the parameter that controls the influence of damage in this disruption is  $a$ , so, we have analyzed in Fig. 11 the influence of this parameter in cortical bone ( $\rho_0 = 2.05 \text{ g/cm}^3$ ) under high constant strain overload ( $\xi = 7\xi_0^*$ ). For high  $a$  values, a small damage level is able to activate remodelling, causing resorption and appropriate damage repairing. Lower  $a$  values reduce bone resorption and consequently damage repairing. Indeed, in the particular case of  $a = 0.0$ , damage does not activate remodelling, so damage repairing would be much slower.

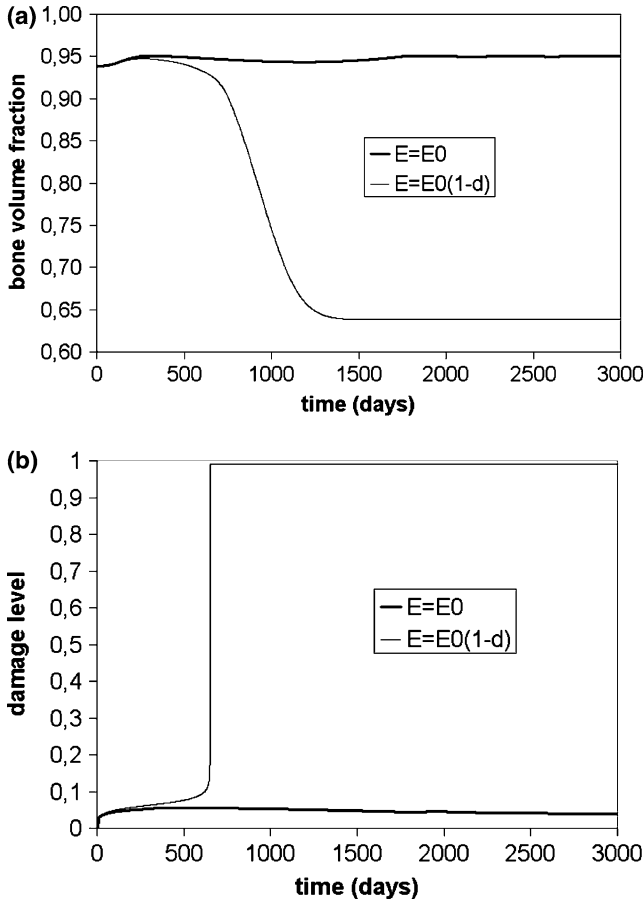


**Fig. 7** Influence of the consideration or not of the elastic modulus degradation in function of the damage level: **a** evolution of the bone volume fraction for cortical bone ( $\rho_0=2.05 \text{ g/cm}^3$ ) under a high overload of constant stress of 34 MPa **b** evolution of damage level under the same loading conditions

### 3.1.5 Influence of the number of loading cycles

The number of loading cycles applied have also a strong influence on the transmitted signal  $s$ , through the mechanical stimulus and damage. We have checked the influence of the number of cycles on the damage evolution and consequently on bone response, keeping constant the mechanical stimulus (strain)  $\bar{\epsilon} = (7\xi_0^*/N^{1/m}) = (7\xi_0^*/10000^{1/4}) = 0.7\xi_0^*$ . In Fig. 12 we see that a greater number of cycles implies higher damage accumulation and consequently higher bone resorption, as expected.

### 3.1.6 Influence of the rate of the equilibrium stimulus adaptation

Two different rates of accommodation have been studied defined by the parameter  $\phi$  in Eq. (15) ( $0.0$  and  $0.002 \text{ days}^{-1}$ ) under disuse conditions and with different focal bone balance parameters ( $f_{bb, \max}=1.0$  and  $f_{bb, \min}=\{1.0;0.8;0.5\}$ ) (see Fig. 13). From these figures we can clearly see how in the case of neutral focal bone

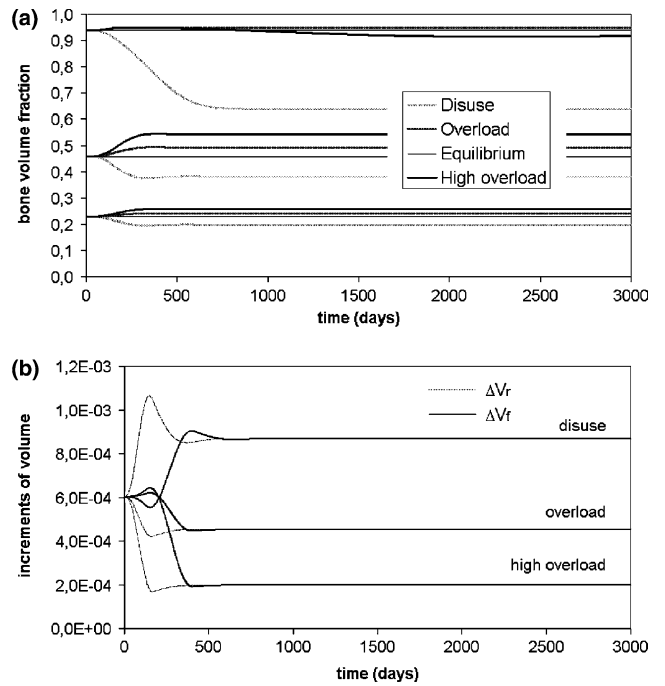


**Fig. 8 a** Evolution of the bone volume fraction for different initial densities,  $\rho_0=2.05, 1.0,$  and  $0.5 \text{ g/cm}^3$  (all with reference to an initial ash fraction of 0.6), and for states of equilibrium  $\xi = \xi_0^*$ , overload  $\xi = 2\xi_0^*$ , high overload  $\xi = 7\xi_0^*$  and disuse  $\xi = 0$ . **b** Evolution of the remodelling increments  $\Delta v_R$  and  $\Delta v_F$  for an initial density of  $1.0 \text{ g/cm}^3$

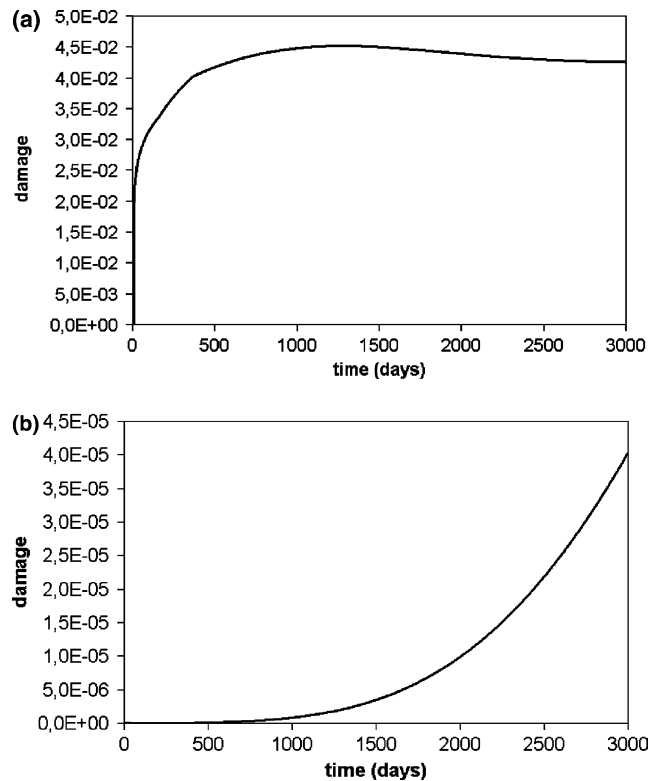


**Fig. 9** Microdamage accumulation under high overload in bones with different initial densities: **a**  $\rho_0=2.05$  and **b**  $\rho_0=1.0 \text{ g/cm}^3$

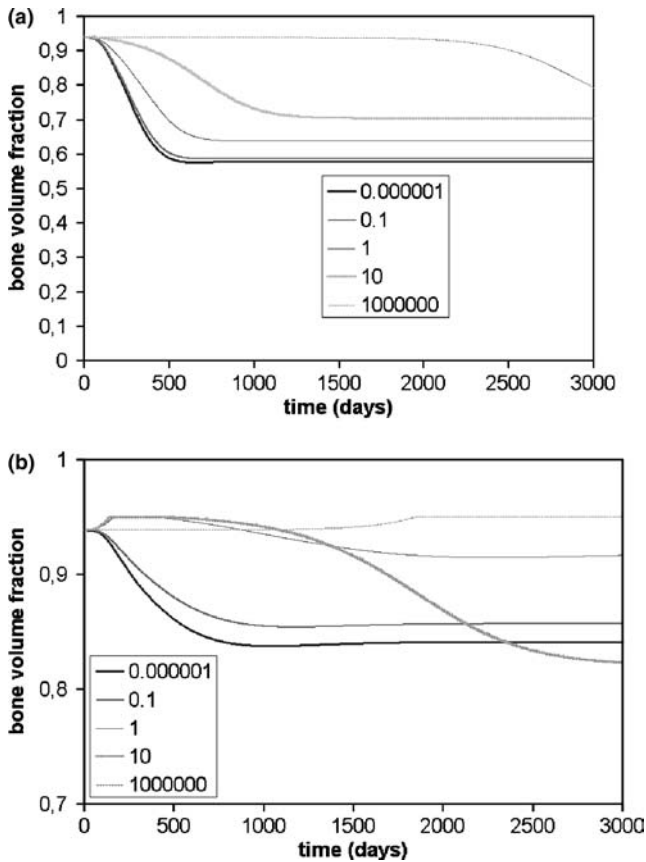


**Fig. 10** Influence of the parameter  $c$  that defines the activation curve as a function of the stimulus  $\xi$  and the damage level  $d$ , under two different loading conditions: disuse (a) and high overload (b)

balance ( $f_{bb, \max} = f_{bb, \min} = 1.0$ ) the influence of the rate of accommodation of the equilibrium stimulus is null, which occurs usually for normal adult bone. This fact could justify why most models that try to simulate bone remodelling of adult bone do not take account the equilibrium stimulus adaptation. However, in the case of growing or old bone, where positive and negative focal bone balance may occur, respectively, the effect of equilibrium stimulus is very important, as was suggested by Turner (1999). Actually, in the case of disuse with null rate of accommodation ( $\xi^* = \xi_0^*$ ) and non-neutral focal bone balance, the asymptotic bone resorption response is reached very slowly as we can see in Fig. 13b. Obviously, the tendency of adaptation is preserved in all cases, whereas it remains a question of time when the dead zone is reached getting remodelling equilibrium. Since there are no experimental results available on cell accommodation, a reasonable value can be chosen by relating the time of convergence of the bone volume fraction with clinical or experimental results. For example, Jaworski and Uthoff (1986) analyzed the effect of long-term immobilization in young dogs, achieving bone volume equilibrium at 480 days, while Li et al. (1990) determined this equilibrium for rats at about 210 days. From Figs. 13 and 14 we can conclude that for constant equilibrium stimulus, it is impossible to

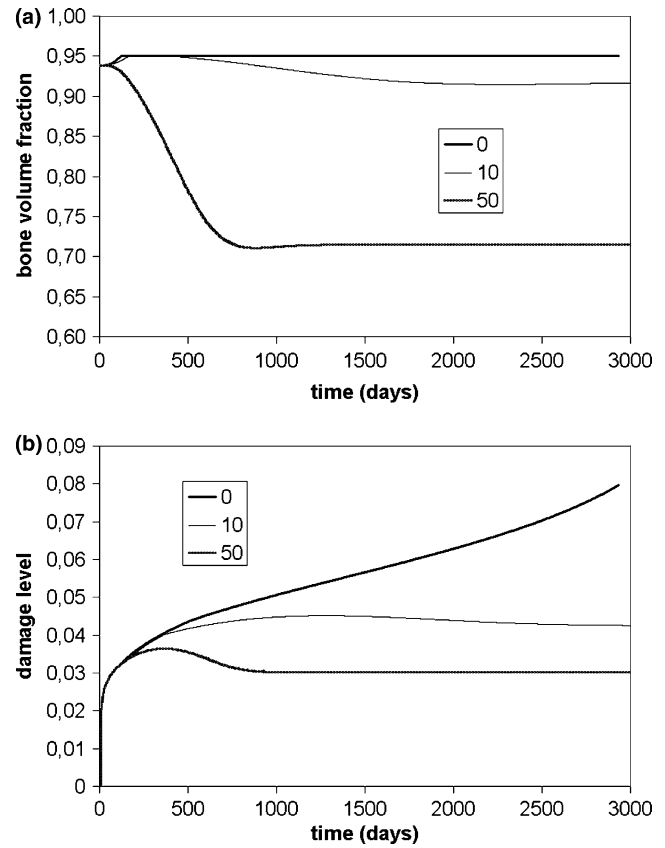


**Fig. 11** Bone volume fraction (a) and damage (b) evolution in cortical bone  $\rho_0 = 2.05 \text{ g/cm}^3$  under high overload ( $\xi = 7\xi_0^*$ ) for different values of  $a = \{0.0; 10.0; 50.0\}$

achieve an asymptotic bone resorption, such as obtained in the experimental works, previously mentioned. On the contrary, when this parameter increases, the equilibrium situation is achieved before, reducing the amount of bone loss in disuse (see Fig. 14). From these results, we can conclude that the rate of equilibrium stimulus adaptation is the parameter with stronger influence in the time that bone needs to achieve the equilibrium state, and that focal bone balance is less important when equilibrium stimulus is not kept constant.

### 3.1.7 Effect of the origination frequency factor $f_{bio}$

Another important parameter is the origination frequency  $f_{bio}$  (recall Eq. 32). It controls the amount of change in bone volume as shown in Fig. 15, where it has been varied between a very low and an unreasonably large value of 0.2, which causes an oscillatory behaviour in the bone response under disuse. Hernandez (2001) assumed a constant value of  $0.0039 \text{ BMUs/mm}^2/\text{day}$  independent of the mechanical stimulus. Frost (1969) measured the activation rate in young people, getting a value of about  $0.055 \text{ BMUs/mm}^2/\text{day}$ ; for ages 30–39 was about  $0.006 \text{ BMUs/mm}^2/\text{day}$  and for 70–89  $0.003 \text{ BMUs/mm}^2/\text{day}$ . In this work, we have assumed  $f_{bio} = 0.03 \text{ BMUs/mm}^2/\text{day}$ , which corresponds to the

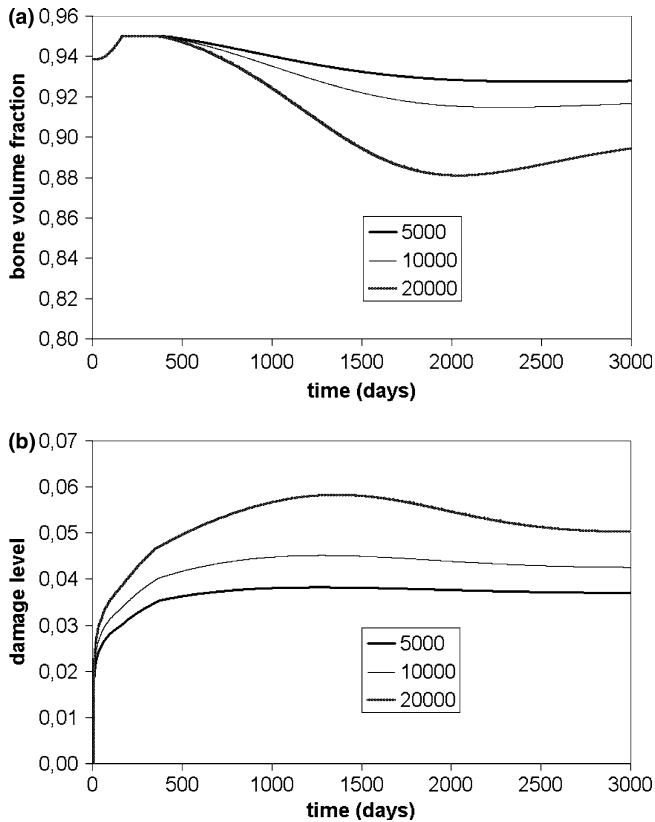


**Fig. 12** Bone volume fraction (a) and damage (b) evolution in cortical bone  $\rho_0 = 2.05 \text{ g/cm}^3$  under high overload ( $\bar{\epsilon} = 7\xi_0^*/N^{1/m} = 7\xi_0^*/10000^{1/4} = 0.7\xi_0^*$ ) applying this stimulus during a different number of cycles 5,000, 10,000 and 20,000

maximum origination frequency that would be activated in complete disuse ( $\xi = 0$ ) or equivalently full damage ( $d = 1$ ). Realistic values of this parameter are not available and present a great variability depending on the age, sex, etc., and therefore, an adjustment of the global behaviour of the model with known clinical or experimental data has still to be performed.

We have analyzed the influence of this factor on cortical bone under a high constant stress overload of 30 MPa. The results obtained are shown in Fig. 16. There, we can observe that, for a higher origination biological factor, bone resorption and damage accumulation are lower. However, for very high values of  $f_{\text{bio}}$  (i.e.  $f_{\text{bio}} = 0.1$  in Fig. 16) bone resorption reduces the mechanical properties, which increases strain and accelerate damage accumulation. This fact actually occurs when a high overload is applied to old cortical bone, with substantial accumulated microdamage; this may accelerate the progression of damage causing bone fracture. The results shown here can help to explain why old bone usually presents a low origination biological factor (Frost 1969).

### 3.1.8 Impact of the secondary mineralization period

In order to fully analyze the effect of the secondary mineralization period, we have studied the case of cortical

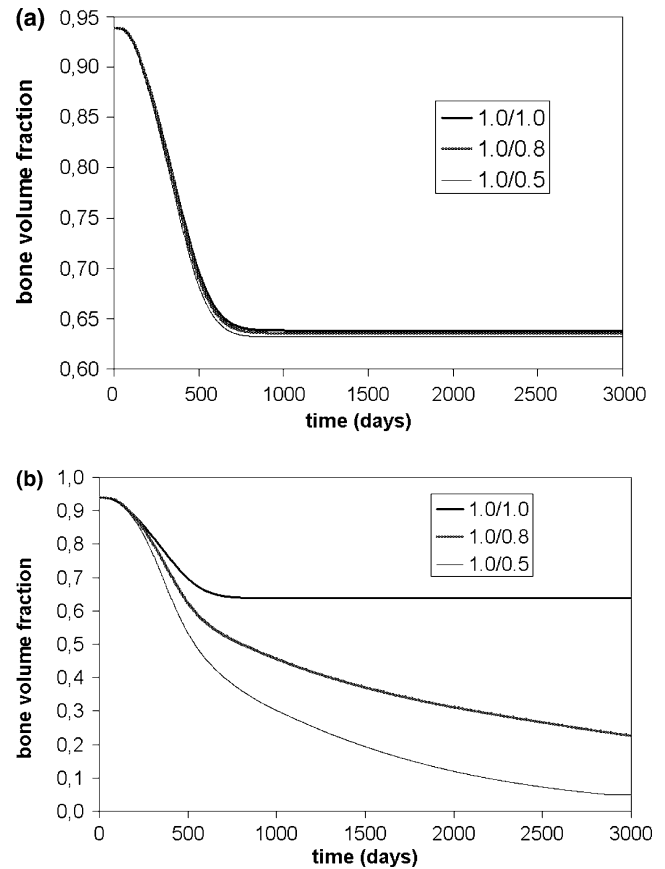


**Fig. 13** Bone volume fraction evolution under disuse for different ratios of focal bone balance  $f_{\text{bb, min}} = \{1.0; 0.8; 0.5\}$  and two rates of the equilibrium stimulus  $\phi$ : **a** 0.002 and **b** 0.0 days<sup>-1</sup>

bone under a high constant stress stimulus. We have defined this period as the interval between the end of the primary mineralization ( $\bar{x} = 0.6$ ) and the point at which the mineral content reaches 95% of the theoretical maximum value, that has been considered here as 0.7. Under these assumptions, we have analyzed the influence of different secondary mineralization periods (16, 9, 6 and

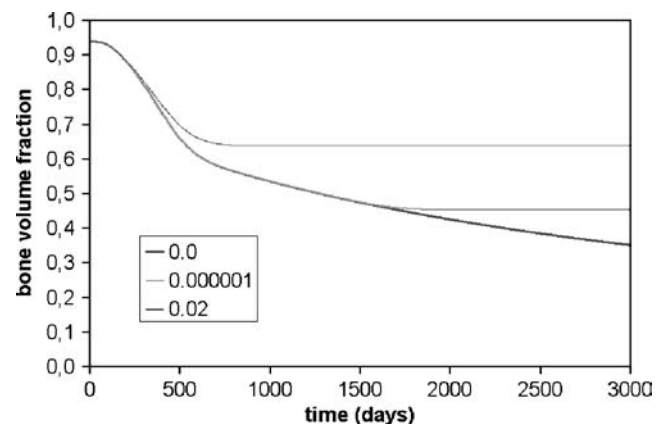


**Fig. 14** Bone volume fraction evolution for different velocities of accommodation  $\phi$  in disuse

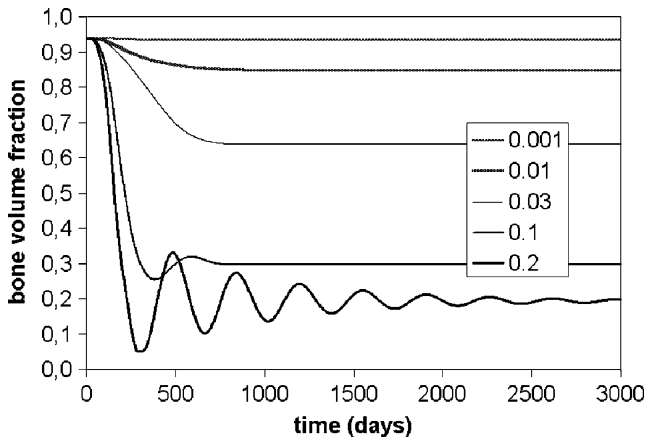
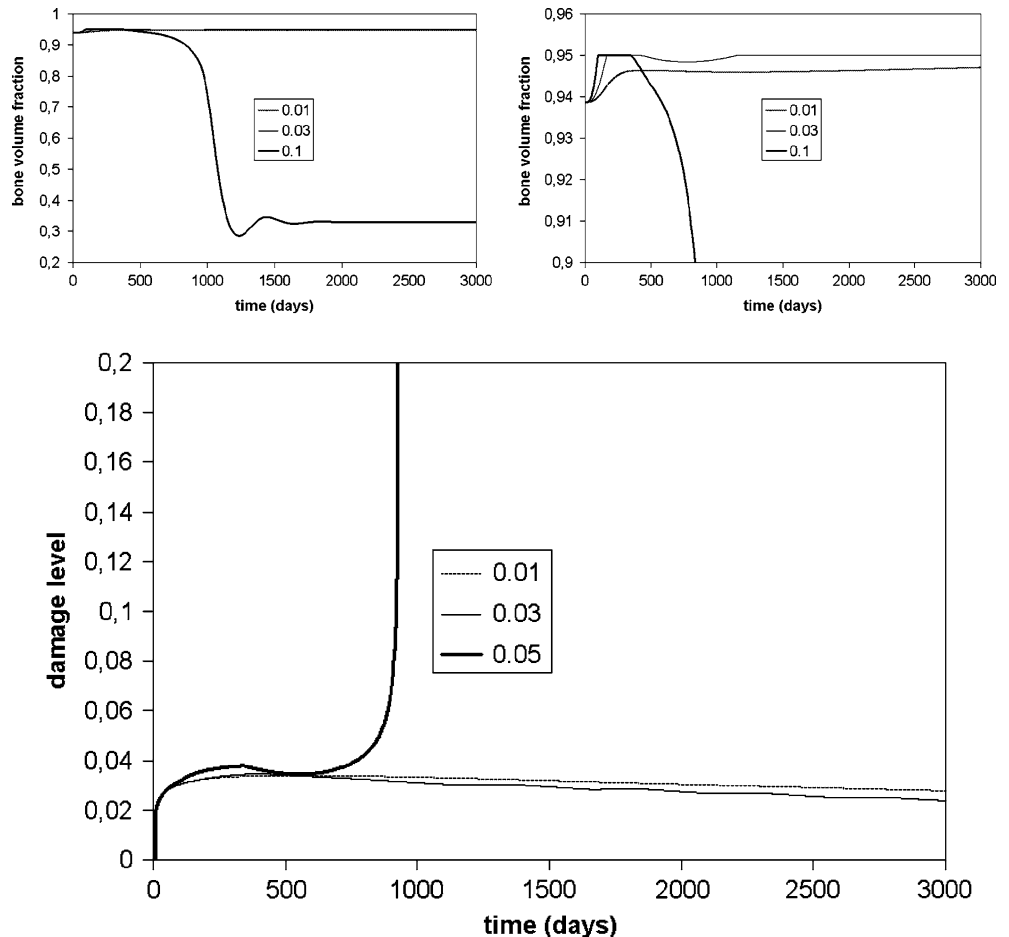


**Fig. 15** Influence of the origination biological factor  $f_{bio}$  in cortical bone loss in disuse

1 years) on bone volume fraction evolution and damage accumulation in cortical bone under a high stress level. We have applied a constant stress of 30 MPa and considered initial conditions of bone volume fraction ( $v^b=0.938$  or equivalently  $\rho=2.05 \text{ g/cm}^3$ ), mineralization ( $\alpha=0.6$ ) and damage ( $d=0.0$ ). Under these conditions, we observe in Fig. 17 that a reduction of the secondary mineralization period decreases the bone resorption caused by micro-damage accumulation. We can also observe in Fig. 17b

**Fig. 16** Bone volume fraction (a) and damage (b) evolution in cortical bone  $\rho_0 = 2.05 \text{ g/cm}^3$  under a constant tension stress of 30 MPa for different origination biological factors



that small periods of secondary mineralization reduce damage accumulation in cortical bone under high overload. Only in the case of a secondary mineralization period of 16 years, damage accumulation is higher than repairing, leading to bone fracture.

### 3.1.9 Differences between tension and compression

All the cases here analyzed have been obtained under tension load. Although we have assumed that bone response is independent of the signal of the strain or stress, we have considered that damage accumulation is different under tension and compression as commented in Eq. 17. In order to study this influence we have applied a constant overload of 34 MPa (both in tension and compression) in cortical bone ( $\rho=2.05 \text{ g/cm}^3$ ). We can see in Fig. 18 how damage under compression grows slower than in tension, producing less bone resorption. Indeed, in this particular example, tension causes failure, whereas compression does not.

### 3.2 THR-prosthesis

FE models of the proximal femur have been used extensively in the context of computer simulations of

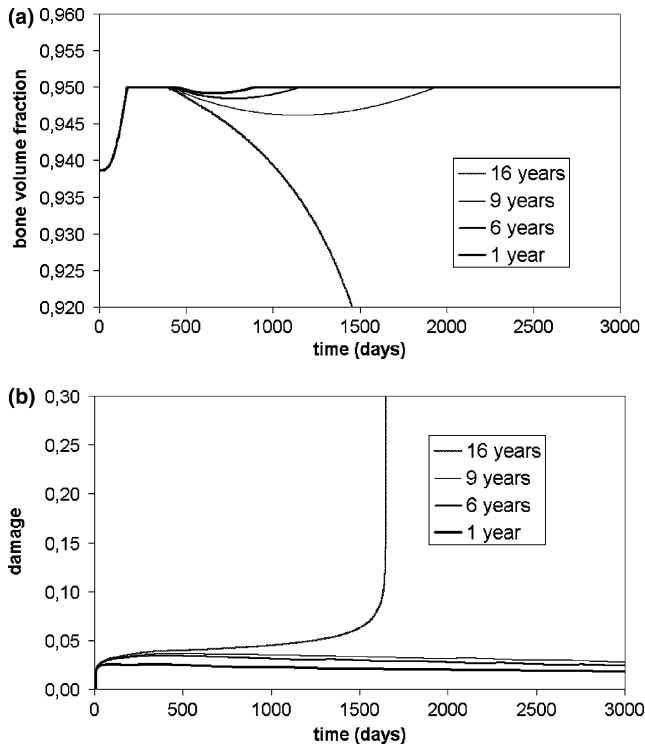


**Fig. 17** Influence of the secondary mineralization period in cortical bone under high overload (constant stress level of 30 MPa). **a** Bone volume fraction evolution and **b** damage accumulation

bone remodelling. Several authors (Carter et al. 1987; Huiskes et al. 1987; Beaupré et al. 1990; Jacobs et al. 1997; Doblaré and García 2002) employed a 2D model with load cases associated to the forces in the gait cycle. Their algorithm provided realistic results after 300 days, starting from a uniform density distribution. Nevertheless, these kinds of models are phenomenological, being unable to predict the real rate of remodelling. The same type of model has been applied to simulate the structural changes after a total hip replacement (THR) with a prosthesis of the Exeter type by Doblaré and García (2001). Although the problem of atrophy in the cortex and the thereby caused reduction in lifetime of the prosthetic device could be predicted, excessive bone resorption appeared in a longer simulation.

The bone remodelling model presented in this paper has been implemented in the user-defined material behavior subroutine (UMAT) in a commercial FE-code ABAQUS 6.3.1 (HKS, Pawtucket, RI). We have used it to accomplish an identical simulation to the one previously discussed (see Fig. 19). It always resulted in a convergent numerical outcome, but our model did not sufficiently approximate the real density distribution. We think that this was caused by the unrealistic characteristics of this simulation. Our computational model simulates bone adaptation from a physiologic and not phenomenological point of view, considering biological and mechanical influences, so it is not able to predict the actual internal bone structure starting from a realistic geometry and a non-real uniform distribu-

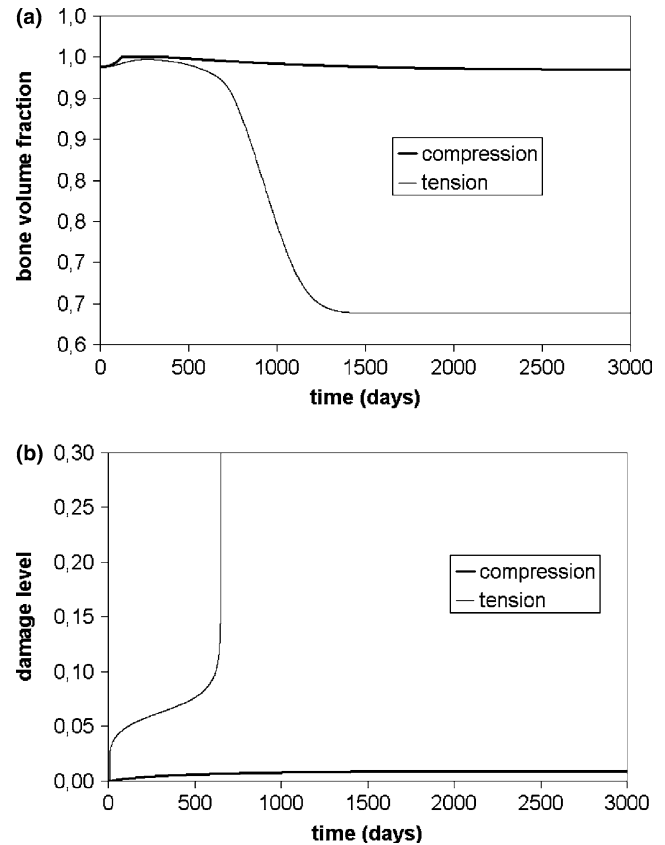


**Fig. 18** Influence of tension and compression stresses (constant level of 34 MPa): **a** bone volume fraction evolution and **b** damage accumulation

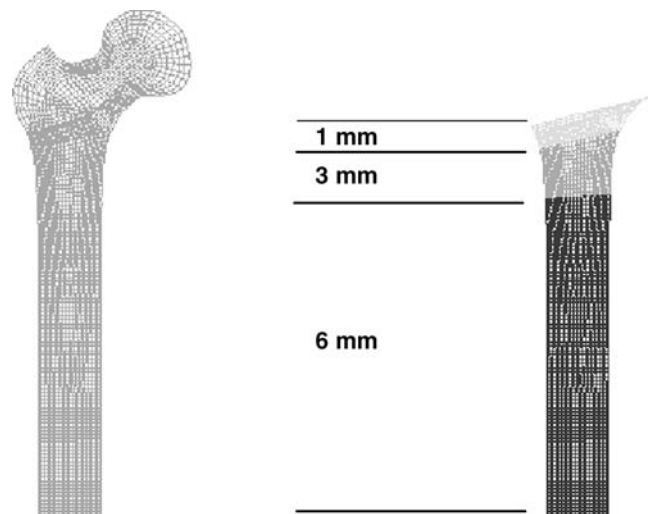


**Fig. 19** FE mesh of the intact femur, and of an additional side plate with different thickness (1, 3 and 6 mm) to connect the cortical layers of the diaphysis (see Jacobs et al. 1997; Jacobs 1994)

tion. Actually, the real internal (and external) structure of the femur or any other bone is not only a product of mechanical adaptation, but is definitely a result of the combination of skeletal growth with the impact of

mechanical, genetic and metabolic factors as well as bone remodelling and modelling. Therefore, simply taking the external shape of a femur with a uniform density distribution cannot lead only by bone remodelling to the real structure. To take this into account, we have solved the same problem but starting from an initial apparent density distribution close to the real one, and checked if our model is able to predict from this distribution an equilibrium state.

We initially used the Stanford model developed by Carter et al. (1987, 1989) for the first 300 days in order to predict a reasonable internal structure. Next, we continued the simulation, but using the model presented here. We can see in Fig. 20 the final bone density distribution with both models, showing that differences are practically undistinguishable.

In the next analysis, after implantation of the Exeter prosthesis (Fig. 21, top) two different simulations were run for different birthrate factors  $f_{\text{bio}} = 0.03$ , and  $0.05$  (see Fig. 22, 23, respectively). In both cases a loss in the upper cortex is clearly observed, being this more pronounced for the bigger value of  $f_{\text{bio}}$  as expected. This bone loss decreases from the proximal to the distal areas.

The amount and location of bone losses are in good correspondence with clinical results (Maloney et al. 2002). As shown in Fig. 24, the mean bone loss observed in various patients after a THR in the lateral and medial cortex is about 20% depending on the site of measurement. Moreover, we found in the numerical simulation minor changes in the bone mass after the second year of the THR, which is very similar to that obtained in clinical observations (Venesmaa et al. 2003).

In order to check the convergence, we have defined the parameter

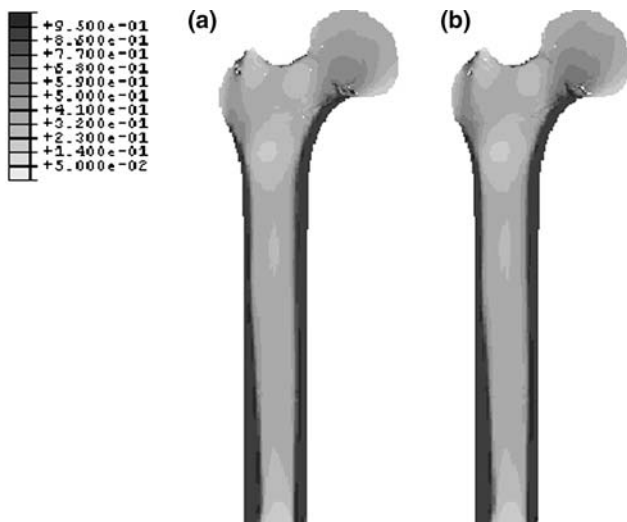


Fig. 20 Bone volume fraction distribution using: **a** the Stanford's model (Beaupré et al. 1990; Jacobs 1994) and **b** the model proposed in this work

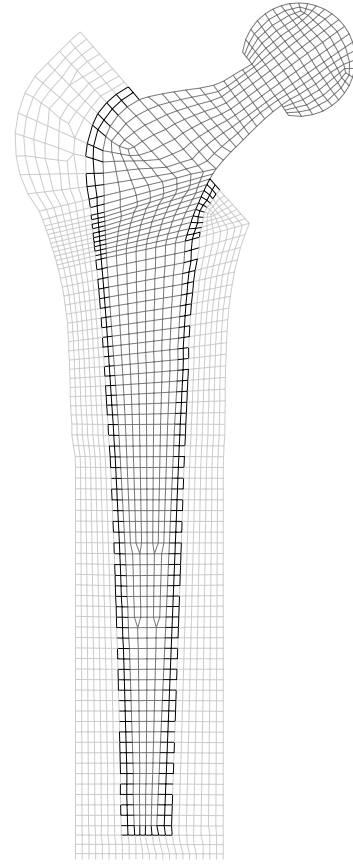


Fig. 21 FE mesh of the prosthesis after implantation in the femur

$$e = \frac{\int_V |\Delta v_b| dV}{\int_V dV} \quad (35)$$

which represents the averaged change in bone volume fraction for each time increment  $\Delta t$ . In Fig. 25 the value of this parameter is depicted for 1,000 days simulations, for the intact femur (with initial density distribution obtained by means of the isotropic Stanford theory) and the THR situation. In the latter case, the parameter  $f_{\text{bio}}$  has been varied in order to estimate its impact on the convergence rate and the final outcome as explained below. After an initial peak, in both cases the convergence parameter tends to a very small value (less than  $1 \times 10^{-6}$  in the first and less than  $1 \times 10^{-5}$  in the second case). A very stable behaviour is achieved without any oscillation. As the convergence curve in Fig. 25 indicates, the structural changes in 1,000 days simulation are hardly observable.

#### 4 Discussion

We have investigated the dynamics of a new damage-repair bone remodelling model, that is able to predict both bone adaptation and stress fractures. It combines concepts from mechanobiological models (Huiskes et al. 2000; Hazelwood et al. 2001; Hernandez 2001; Hernan-



**Fig. 22** Bone volume fraction distribution in the femur for a birthrate factor of  $f_{\text{bio}} = 0.03$  after: **a** 330, **b** 660 and **c** 990 days of implantation

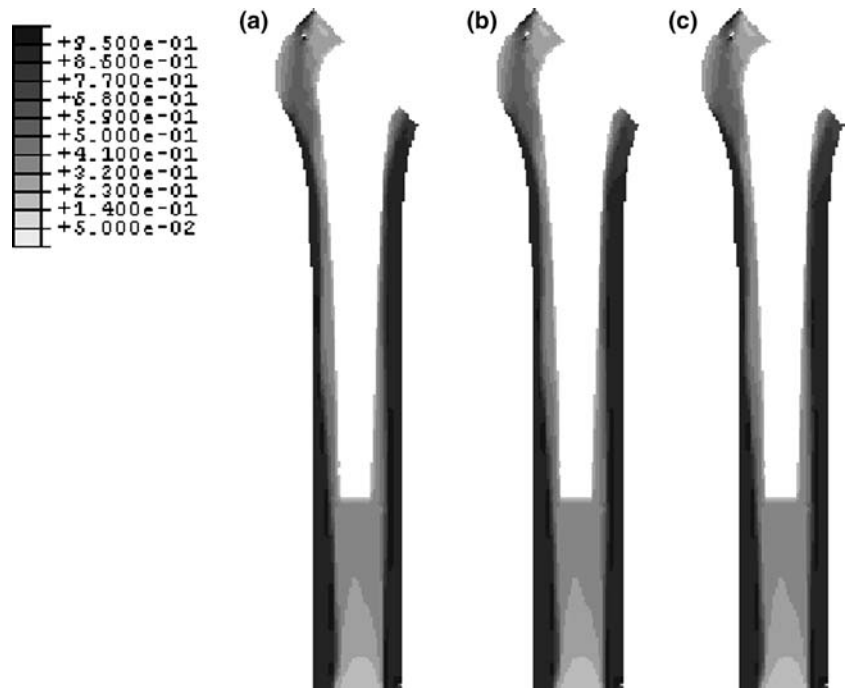
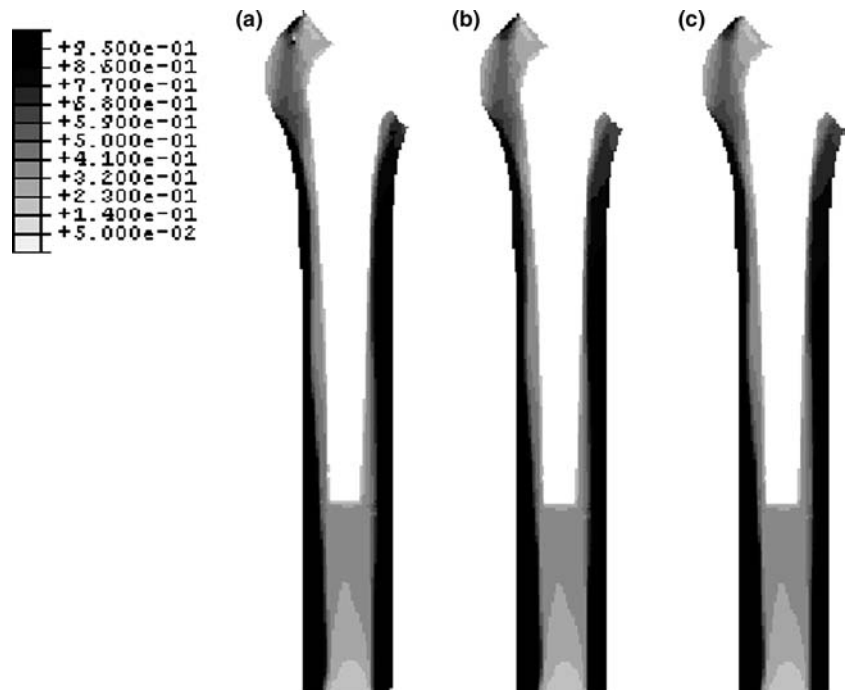


**Fig. 23** Bone volume fraction distribution in the femur for a birthrate factor of  $f_{\text{bio}} = 0.05$  after: **a** 330, **b** 660 and **c** 990 days of implantation



dez et al. 2000, 2003) with others related to the prediction of the mechanical failure of bone in laboratory experiments (Burr et al. 1998; Davy and Jepsen 2001; Lee et al. 2000; Pattin et al. 1996). Most of the available mechanobiological models are based on bone adaptation to the mechanical environment, but do not take into account that actual damage can accumulate faster than remodelling can repair it, producing a stress fracture.

Actually, Huiskes et al. (2000) proposed a model that includes a separate description of osteoclastic resorption and osteoblastic formation governed by mechanical factors. A biological osteocyte mechanosensory system was employed as the basis of their mechanobiological bone remodelling model. They obtained reasonable results that allow to explain the effects of mechanical load on bone trabecular structure.

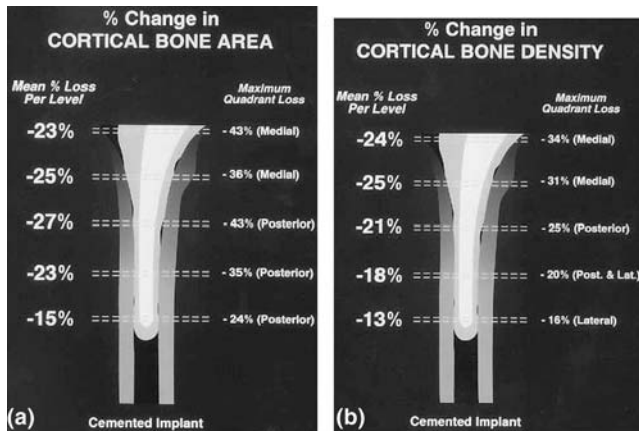


**Fig. 24** Changes in bone area (a) and density (b) due to a THR (taken with permission from Maloney et al. 2002)

Hazelwood et al. (2001) developed a model of mechanical adaptation with metabolic items. In it, BMUs are activated in response to either disuse or microdamage. Although this model supposed an important advance in understanding bone remodelling, it contains some limitations. For instance, it does not consider the 3D geometry of the BMU (only a 2D approximation was used). Moreover, the process of mineral accumulation in newly osteoid bone, which plays an important role in bone remodelling as many authors have pointed out (Hernandez et al. 2001), was not taken into account. Additionally, the influence of damage on the macroscopic stiffness was also neglected, which itself alters the remodelling process. Apart from these theoretical items, the model was only applied to simulate the porosity increase in cortical bone.

Hernandez (2001) and Hernandez et al. (2000, 2003) proposed a computational model of bone remodelling that considers the complete activity of BMUs from a 3D point of view and accounts for changes in the degree of mineralization of bone tissue. Measurements taken from histomorphometric studies of human bone were used to represent the rate of appearance, shape, rate of pro-

gression and lifespan of BMUs as well as the time periods during which bone is resorbed and formed at each individual remodelling site. Although this model also implied a significant advance in the comprehension and simulation of the remodelling process, it is certainly restricted. The theoretical formulation of this model considers a mechanical stimulus (Hernandez 2001; Hernandez et al. 2000) which was not employed in the numerical analyses. Furthermore, the impact of cumulative microdamage was neglected despite its significance (Prendergast and Taylor 1994; Hazelwood et al. 2001; Martin 2003a, b; Martin et al. 1998).

The only theoretical model that tries to simulate the growth and repair of microdamage in bone has been developed by Taylor and Lee (2003). However, their model requires a significant amount of computer power since they follow the growth of each crack individually. In fact, it does not allow to simulate the bone adaptation process in an entire bone. Moreover, they do not take into account bone resorption by disuse, which is one of the most significant features of bone adaptation (Takata and Yasui 2001; Jaworski and Uthoff 1986; Gross and Rubin 1995).

The model proposed in this work is an extension of the previously cited. It takes into account both biological (BMUs activity) and mechanical (microdamage accumulation and mechanical properties degradation) influences. The main assumption that we propose is that bone adaptive response (by means of BMUs activity) is activated by disuse or removal of actual microdamage.

Nowadays, there are many algorithms that have been formulated to mimic the adaptive property of bone. Actually, John Currey (1995) indicated that a computational model should be testable to check if its predictions are at least as good as those of other models. In this sense, we consider the model here proposed improves previous ones, because it is an extension that incorporates most of the relevant effects in bone remodelling. Bone resorption due to low load, bone formation due to high load, bone loss for high loads reducing microdamage. Stress fracture for high loads that induce microdamage to grow faster than repair has

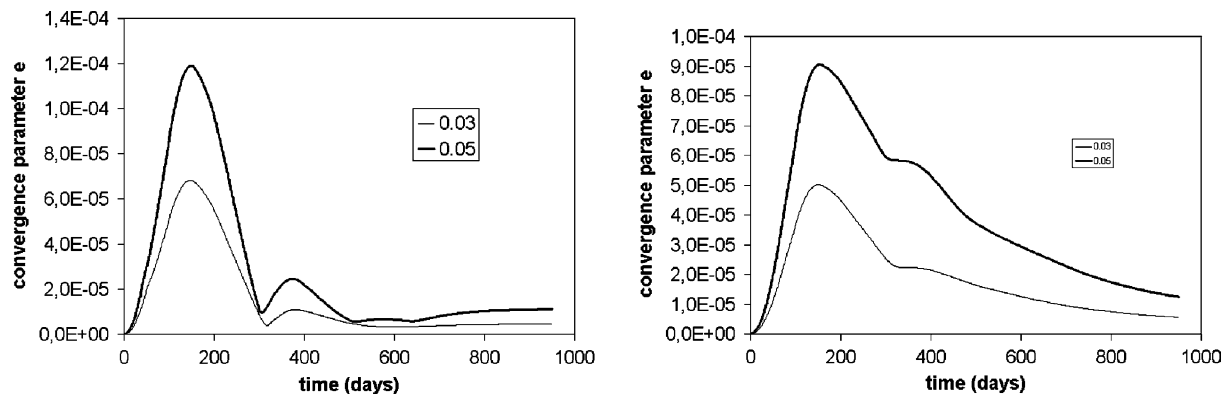


**Fig. 25** Convergence parameter as introduced in Eq. 35 for the intact femur (left), where the method was applied on the initial internal structure predicted by the Stanford algorithm, and for a THR with the EXETER prosthesis for various  $f_{bio}$

been also considered, as well as the influence of mineralization. Bone is always remodelling even if equilibrium is achieved (and thus, is never hypermineralized). In addition more specific conclusions have been obtained from this work:

- Loss of material stiffness has to be included in these kinds of models, because it can cause an important stress/strain redistribution, being crucial in the prediction of fatigue fractures.
- High overload in cortical bone causes more bone resorption than in trabecular bone.
- If damage does not activate remodelling, damage repairing would be much slower.
- Increasing the number of cycles causes more damage and consequently more bone resorption.
- If the focal bone balance is neutral, the rate of the equilibrium stimulus adaptation has small influence on the final bone response.
- If the rate of the equilibrium stimulus adaptation is null, the focal bone balance has important consequences. When the equilibrium stimulus is adaptive the influence of the focal bone balance is reduced depending on the rate that this stimulus accommodates.
- A higher origination frequency factor ( $f_{\text{bio}}$ , biological factor) helps to repair quicker damage, resorbing bone faster. But if this value is very high or initial damage level is very high it can accelerate the appearance of a bone fracture.
- Short secondary mineralization periods accelerate the process of damage repair and therefore prevents the appearance of stress fractures.
- Damage accumulation in tension and compression are different, producing therefore a different bone response.
- From the second year after THA we found minor losses in bone mass, which is very similar to clinical studies (Venesmaa et al. 2003).

Nevertheless, this model also presents some simplifications and limitations that have to be discussed with respect to the conclusions obtained. First, we have considered a different bone response under tension and compression as consequence of well-known differences between damage accumulation in tension and compression (Pattin et al. 1996), but we do not have taken into account this effect in the mechanical stimulus  $\xi$  that controls bone response, which could exist. This model has been applied to simulate bone adaptation in the interior of bone tissue, however, in the case of cortical bone, most of the process is produced by periosteal or endosteal remodelling, effect that has not been considered in this work. It is also well-known that cortical and trabecular bone are anisotropic (Martin et al. 1998; Currey 2002). Here, as a first step, we have considered an isotropic spatial distribution of pores, bone mineralization and damage. Furthermore, anisotropy in each type of bone is induced by different effects. In cortical

bone, porosity is very low and anisotropy is mainly controlled by the lamellar and osteonal orientations. On the contrary, in trabecular bone, porosity is higher and anisotropy is mainly determined by the trabecular orientation. In a future work anisotropy should be included considering both effects.

The mechanism that activates remodelling, that is BMU origination, is not fully clear yet. The point in which different authors agree is that osteocytes are the best candidates to detect changes in strain and micro-damage. They would transmit a biochemical, electrical or any other type of signal to the lining cells (Parfitt 1996), inhibitory (Martin 2000) or not (Parfitt 1996). Although we have assumed here that this signal is inhibitory, it would not be an important problem to modify it in our model, making it non-inhibitory. However, it is even more important to know how this signal is induced by strain and microdamage. Indeed, we have assumed that both effects control it by a mechanism defined by the expression (33). This assumption, although able to predict a number of important phenomena, as has been pointed out, needs additional research.

Although this model includes many parameters, all can be experimentally measured and have been obtained from available literature. Nevertheless, we have also to take into account that their value may be also influenced by factors such as age, sex, growth factors (Komarova et al. 2003) and different clinical treatments (parathyroid hormone (Lane et al. 1998), biphosphonates (Hazelwood et al. 2004; Hughes et al. 1995; Parfitt et al. 1996)). For example, it is known that bone remodelling increases under sex steroid deficiency, causing the birth of new BMUs or the prolongation of the life span of the already existing (Manolagas 2000). All these features can be simply analyzed by appropriately modifying the value of the associated parameters. In fact, similar models have been used to study the influence of an alendronate treatment, uniquely modifying the secondary mineralization period (Hernandez et al. 2001).

In conclusion, the theoretical bone remodelling model here presented implies, in our opinion, an advance in the understanding of the adaptation of bone tissue under different biological and mechanical conditions. In the future, it could be used with clinical purposes for applications such as programming the personalized best activities to increase bone mass without risk of fracture, the reduction of the long-term risk of stress fracture in some specific activities, the evolution of bone quality after orthopaedic treatments, the evolution and treatment of osteoporosis, etc.

---

## References

- Wolff J (1986) *The Law of Bone Remodelling Das Gesetz der Transformation der Knochen*, Kirschwald, 1892 Translated by Maquet P, Furlong R. Springer, Berlin

- Cowin SC (2001) The false premise in Wolff's Law. In: Bone mechanics handbook, 2nd edn, chap. 30, CRC Press, Boca Raton, pp 30-1-30-15
- Huiskes R, Weinans H, Grootenboer HJ, Dalstra M, Fudala B, Sloof TJ (1987) Adaptive bone-remodelling theory applied to prosthetic-design analysis. *J Biomech* 20(11/12):1135-1150
- Carter DR, Fyhrie DP, Whalen RT (1987) Trabecular bone density and loading history: regulation of tissue biology by mechanical energy. *J Biomech* 20:785-795
- Carter DR, Orr TE, Fyhrie DP (1989) Relationships between loading history and femoral cancellous bone architecture. *J Biomech* 22(3):231-244
- Prendergast PJ, Taylor D (1994) Prediction of bone adaptation using damage accumulation. *J Biomech* 27:1067-1076
- Martin RB (1995) A mathematical model for fatigue damage repair and stress fracture in osteonal bone. *J Orthop Res* 13:309-316
- Jacobs CR, Simo JC, Beaupré GS, Carter DR (1997) Adaptive bone remodeling incorporating simultaneous density and anisotropy considerations. *J Biomech* 30(6):603-613
- Hart RT, Fritton SP (1997) Introduction to finite element based simulation of functional adaptation of cancellous bone. *Forma* 12:277-299
- Fernandes P, Rodrigues H, Jacobs CR (1999) A model of bone adaptation using a global optimisation criterion based on the trajectorial theory of wolf. *Comput Methods Biomed Engin* 2(2):125-138
- Doblaré M, García JM (2002) Anisotropic bone remodelling model based on a continuum damage-repair theory. *J Biomech* 35(1):1-17
- Doblaré M, García JM (2001) Application of an anisotropic bone-remodelling model based on a damage-repair theory to the analysis of the proximal femur before and after total hip replacement. *J Biomech* 34(9):1157-1170
- Cowin SC, Hegedus DH (1976) Bone remodeling i: a theory of adaptive elasticity. *J Elasticity* 6:313-326
- Hart RT, Davy DT, Heiple KG (1984) A computational model for stress analysis of adaptive elastic materials with a view toward applications in strain-induced bone remodelling. *J Biomech Engin* 106:342-350
- Beaupré GS, Orr TE, Carter DR (1990) An approach for time-dependent bone modeling and remodeling-theoretical development. *J Orthop Res* 8(5):651-661
- Weinans H, Huiskes R, Grootenboer HJ (1992) The behavior of adaptive bone-remodeling simulation models. *J Biomech* 25:1425-1441
- Cowin SC (1986) Wolff's law of trabecular architecture at remodeling equilibrium. *J Biomech Eng* 108(1):83-88
- Luo GM, Cowin SC, Sadegh AM (1992) An evolutionary wolf's law for trabecular architecture. *J Biomech Eng* 114(1):129-136
- Ramtani S, Zidi M (2001) A theoretical model of the effect of continuum damage on a bone adaptation model. *J Biomech* 34(4):471-479
- Doblaré M, Ramtani S, García JM (2004) Computer simulation of an adaptive damage-bone remodeling law applied to three unit-bone bars structure. *Comput Biol Med* 34(3):259-273
- Hart RT (2001) Bone modeling and remodeling: theories and computation. In: Bone mechanics handbook, 2nd edn, chap 31, CRC Press, Boca Raton, pp 31-1-31-42
- Petermann HE, Reiter TJ, Rammerstorfer FG (1997) Computational simulation of internal bone remodeling. *Arch Comput Meth Eng* 4(4):295-323
- Huiskes R, Ruimerman R, GH van Lenthe, Janssen JD (2000) Effects of mechanical forces on maintenance and adaptation of form in trabecular bone. *Nature* 405:704-706
- Hazelwood SJ, Martin RB, Rashid MM, Rodrigo JJ (2001) A mechanistic model for internal bone remodeling exhibits different dynamic responses in disuse and overload. *J Biomech* 34:299-308
- Hernandez CJ (2001) Simulation of bone remodeling during the development and treatment of osteoporosis. PhD thesis, Stanford University, Stanford, CA
- Hernandez CJ, Beaupré GS, Carter DR (2000) A model of mechano-biologic and metabolic influences on bone adaptation. *J Rehabil Res Dev* 37(2):235-244
- Taylor D, Lee TC (2003) Microdamage and mechanical behaviour: predicting failure and remodelling in compact bone. *J Anat* 203:203-211
- Taylor D, Casolari E, Bignardi C (2004) Predicting stress fractures using a probabilistic model of damage, repair and adaptation. *J Orthop Res* 22(3):487-494
- Hernandez CJ, Beaupré GS, Marcus R, Carter DR (2001) A theoretical analysis of the contributions of remodeling space, mineralization, and bone balance to changes in bone mineral density during alendronate treatment. *Bone* 29(6):511-516
- Hernandez CJ, Beaupré GS, Keller TS, Carter DR (2001) The influence of bone volume fraction and ash fraction on bone strength and modulus. *Bone* 29(1):74-78
- Burr DB, Turner CH, Naick P, Forwood MR, Ambrosius W, Hasan MS, Pidaparti R (1998) Does microdamage accumulation affect the mechanical properties of bone? *J Biomech* 31(4):337-345
- Jepsen KJ, Davy DT, Akkio O (2001) Observations of damage in bone. In: Bone mechanics handbook, 2nd edn, chap 17, CRC Press, Boca Raton, pp 17-1-17-18
- Davy DT, Jepsen KJ (2001) Bone damage mechanics. In: Bone mechanics handbook, 2nd edn, chap 18, CRC Press, Boca Raton, pp 18-1-18-25
- Pattin CA, Caler WE, Carter DR (1996) Cyclic mechanical property degradation during fatigue loading of cortical bone. *J Biomech* 29(1):69-79
- Zioupos P, Currey JD (1998) Changes in the stiffness, strength, and toughness of human cortical bone with age. *Bone* 22(1):57-66
- Lemaitre J, Chaboche JL (1990) Mechanics of solid materials. Cambridge University Press, Cambridge
- Simo JC, Ju JW (1987) Strain and stress-based continuum damage models: formulation. *Int J Solids Struct* 23(7):821-840
- Keller TS (1994) Predicting the compressive mechanical behavior of bone. *J Biomech* 27(9):1159-1168
- Martin RB, Burr DR, Sharkey NA (1998) Skeletal tissue mechanics. Springer, Berlin Heidelberg New York
- Frost HM (1964) Dynamics of bone remodelling. In: Bone biodynamics. Little Brown Co, Boston, pp 315-333
- Rubin C, Turner AS, Bain S, Mallinckrodt C, McLeod K (2001) Low mechanical signals strengthen long bones. *Nature* 412:603-604
- Carter DR, Beaupré GS (2001) Skeletal function and form. Cambridge University Press, Cambridge
- Mikic B, Carter DR (1995) Bone strain gage data and theoretical models of functional adaptation. *J Biomech* 28(4):465-469
- Whalen RT, Carter DR, Steele CR (1988) Influence of physical activity on the regulation of bone density. *J Biomech* 21(10):825-837
- Jacobs CR (1994) Numerical simulation of bone adaptation to mechanical loading. PhD thesis, Stanford University, Stanford, CA
- Carter DR (1984) Mechanical loading histories and cortical bone remodeling. *Calcif Tissue Int* 36:S19-S24
- Tsubota K, Adachi T, Tomita Y (2002) Functional adaptation of cancellous bone in human proximal femur predicted by trabecular surface remodeling simulation toward uniform stress state. *J Biomech* 35(12):1541-1551
- Turner CH (1999) Toward a mathematical description of bone biology: the principle of cellular accommodation. *Calcif Tissue Int* 65(6):466-471
- Zioupos P, Currey JD (1998) Cumulative damage and the response of human bone in two-step loading fatigue. *J Biomech* 31:825-833
- Lee TC, FJ O'Brien, Taylor D (2000) The nature of fatigue damage in bone. *Int J Fatigue* 22:847-853
- Parfitt AM (1983) The physiologic and clinical significance of bone histomorphometric data. In: Bone histomorphometry techniques and interpretation. CRC Press, Boca Raton, pp 143-223

- Martin RB (1984) Porosity and specific surface of bone. In: *Critical reviews in biomedical engineering*, vol 10, chap 3, CRC Press, Boca Raton, pp 179–222
- Gross TS, Rubin CT (1995) Uniformity of resorptive bone loss induced by disuse. *J Orthop Res* 13(5):708–714
- Li XJ, Jee WS, Chow SY, Woodbury DM (1990) Adaptation of cancellous bone to aging and immobilization in the rat: a single photon absorptiometry and histomorphometry study. *Anat Rec* 227(1):12–24
- Takata S, Yasui N (2001) Disuse osteoporosis. *J Med Invest* 48(3–4):147–156
- ZFG Jaworski, Uthoff HK (1986) Reversibility of nontraumatic disuse osteoporosis during its active phase. *Bone* 7:431–439
- Martin RB (2003a) Fatigue microdamage as an essential element of bone mechanics and biology. *Calcif Tissue Int* 73(2):101–107
- Martin RB (2003b) Fatigue damage, remodeling, and the minimization of skeletal weight. *J Theor Biol* 220(2):271–276
- Bentolila V, Boyce TM, Fyhrle DP, Drumb R, Skerry TM, Schaffler MB (1990) Intracortical remodeling in adult rat long bones after fatigue loading. *J Orthop Res* 8(5):651–661
- Mori S, Burr DB (1993) Increased intracortical remodeling following fatigue damage. *Bone* 14(2):103–109
- Verborgt O, Gibson GJ, Schaffler MB (2000) Loss of osteocyte integrity in association with microdamage and bone remodeling after fatigue in vivo. *J Bone Miner Res* 15:60–67
- Martin RB (2000) Toward a unifying theory of bone remodeling. *Bone* 26(1):1–6
- Cowin SC, Moss ML (2001) Mechanosensory mechanisms in bone. In: *Bone mechanics handbook*, 2nd edn, chap 29, CRC Press, Boca Raton, pp 29–1–29–17
- Noble B (2003) Bone microdamage and cell apoptosis. *Eur Cell Mater* 21(6):46–55
- Taylor D, Hazenberg JG, Lee TC (2003) The cellular transducer in damage-stimulated bone remodelling: a theoretical investigation using fracture mechanics. *J Theor Biol* 225(1):65–75
- Frost HM (1969) Tetracycline-based histological analysis of bone remodelling. *Calcif Tissue Res* 3:211–237
- Maloney WJ, Schmalzried T, Harris WH (2002) Analysis of long-term cemented total hip arthroplasty retrievals. *Clin Orthop* 405:70–78
- Venesmaa PK, Kroger HP, Jurvelin JS, Miettinen HJ, Suomalainen OT, and Alhava EM (2003) Periprosthetic bone loss after cemented total hip arthroplasty: a prospective 5-year dual energy radiographic absorptiometry study of 15 patients. *Acta Orthop Scand* 74(1):31–36
- Hernandez CJ, GS Beaupré, Carter DR (2003) A theoretical analysis of the changes in basic multicellular unit activity at menopause. *Bone* 32:357–363
- Currey JD (1995) The validation of algorithms use to explain adaptive remodeling in bone. In: *Bone structure and remodeling*. World Scientific, Singapore, pp 9–13
- Currey JD (2002) *Bones Structure and mechanics*. Princeton University Press, New Jersey
- Parfitt AM (1996) Skeletal heterogeneity and the purposes of bone remodeling: implications for the understanding of osteoporosis. In: *Osteoporosis*, vol 1. Academic Press, New York
- Komarova SV, Smith RJ, Dixon SJ, Sims SM, Wahl LM (2003) Mathematical model predicts a critical role for osteoclast autocrine regulation in the control of bone remodeling. *Bone* 33(2):206–215
- Lane NE, Sanchez S, Modin GW (1998) Parathyroid hormone treatment can reverse corticosteroid-induced osteoporosis. *J Clin Invest* 102:1627–1633
- Hazelwood SJ, Martin RB, Nyman JS, Yeh OC (2004) A theoretical analysis of long-term bisphosphonate effects on trabecular bone volume and microdamage. *Bone* 35:296–305
- Hughes DE, Wright KR, Uy HL, Sasaki A, Yoneda T, Roodman GD, Mundy GR, Boyce BF (1995) Bisphosphonates promote apoptosis in murine osteoclasts in vitro and in vivo. *J Bone Miner Res* Oct 10(10):1478–1487
- Parfitt AM, Mundy GR, Roodman GD, Hughes DE, Boyce BF (1996) A new model for the regulation of bone resorption, with particular reference to the effects of bisphosphonates. *J Bone Miner Res* 11(2):150–159
- Manolagas SC (2000) Birth and death of bone cells: basic regulatory mechanisms and implications for the pathogenesis and treatment of osteoporosis. *Endocr Rev* 21(2):115–137